Title

Vascular HIF2 Signaling Prevents Cardiomegaly, Alveolar Congestion, and Capillary Remodeling During Chronic Hypoxia

Journal

Arteriosclerosis Thrombosis and Vascular Biology, 45(3)

ISSN

1079-5642

Authors

Albendea-Gomez, Teresa
Mendoza-Tamajon, Susana
Castro-Mecinas, Rosana
et al.

Publication Date

2025-03-01

DOI

10.1161/atvbaha.124.321780

Peer reviewed

Arteriosclerosis, Thrombosis, and Vascular Biology

BASIC SCIENCES

Vascular HIF2 Signaling Prevents Cardiomegaly, Alveolar Congestion, and Capillary Remodeling During Chronic Hypoxia

Teresa Albendea-Gomez, Susana Mendoza-Tamajon, Rosana Castro-Mecinas, Beatriz Escobar, Susana Ferreira Rocha, Sonia Urra-Balduz, Jose Angel Nicolas-Avila, Eduardo Oliver, Maria Villalba-Orero, Silvia Martin-Puig

BACKGROUND: Hypoxia is associated with the onset of cardiovascular diseases including cardiac hypertrophy and pulmonary hypertension. HIF2 (hypoxia inducible factor 2) signaling in the endothelium mediates pulmonary arterial remodeling and subsequent elevation of the right ventricular systolic pressure during chronic hypoxia. Thus, novel therapeutic opportunities for pulmonary hypertension based on specific HIF2 inhibitors have been proposed. Nevertheless, HIF2 relevance beyond the pulmonary endothelium or in the cardiac adaptation to hypoxia remains elusive. Wt1 (Wilms tumor 1) lineage contributes to the heart and lung vascular compartments, including pericytes, endothelial cells, and smooth muscle cells.

METHODS: Here, we describe the response to chronic hypoxia of a novel HIF2 mutant mouse model in the Wt1 lineage (*Hif2/Wt1* cKO [conditional knockout]), characterizing structural and functional aspects of the heart and lungs by means of classical histology, immunohistochemistry, flow cytometry, echocardiography, and lung ultrasound analysis.

RESULTS: *Hif2/Wt1* cKO is protected against pulmonary remodeling and increased right ventricular systolic pressure induced by hypoxia, but displays alveolar congestion, inflammation, and hemorrhages associated with microvascular instability. Furthermore, lack of HIF2 in the Wt1 lineage leads to cardiomegaly, capillary remodeling, right and left ventricular hypertrophy, systolic dysfunction, and left ventricular dilation, suggesting pulmonary-independent cardiac direct roles of HIF2 in hypoxia. These structural defects are partially restored upon reoxygenation, while cardiac functional parameters remain altered.

CONCLUSIONS: Our results indicate that cardiopulmonary HIF2 signaling prevents excessive vascular proliferation during chronic hypoxia and define novel protective roles of HIF2 to warrant stable microvasculature and organ function.

GRAPHIC ABSTRACT: A graphic abstract is available for this article.

Key Words: diagnostic imaging ■ heart failure ■ hypoxia ■ microvessels ■ oxygen ■ pulmonary hypertension ■ Wilms tumor 1

Low oxygen tensions induce the activation of HIFs (hypoxia inducible factors) that are heterodimeric transcription factors composed by an oxygen-regulated α-subunit and a constitutively expressed oxygen-independent β-subunit, also known as ARNT (aryl hydrocarbon receptor nuclear translocator).[1] In normal oxygen conditions or normoxia, the proline residues of HIFα subunits are hydroxylated by oxygen-dependent PHDs (prolyl-4-hydroxylases). The VHL (von Hippel-Lindau) protein binds to hydroxylated HIFα and acts as a substrate recognition component of the E3 ubiquitin ligase complex, which leads to proteosomal degradation of the HIFα protein. Under hypoxia, the activity of PHDs is suppressed, and HIFα subunits translocate into the nucleus to bind HIF1β. Then, the heterodimer HIFα/HIFβ binds to the hypoxia response elements in its target genes, resulting in their transcriptional activation.[2–4] There are 2 main HIFα isoforms with transcriptional capacity. HIF1 is known to be associated with the upregulation of glycolytic genes such as GLUT1

Correspondence to: Silvia Martin-Puig, PhD, Instituto de Investigaciones Biomedicas Sols-Morreale (IIBM), CSIC-UAM, C/Arturo Duperier 4, 28029 Madrid, Spain. Email smpuig@iib.uam.es

Supplemental Material is available at https://www.ahajournals.org/doi/suppl/10.1161/ATVBAHA.124.321780.
For Sources of Funding and Disclosures, see page e96.

Arterioscler Thromb Vasc Biol is available at www.ahajournals.org/journal/atvb

Nonstandard Abbreviations and Acronyms

ARNT	aryl hydrocarbon receptor nuclear translocator
AT/ET	acceleration time to ejection time pulmonary
CSPG	chondroitin sulfate proteoglycan 4
cKO	conditional knockout
DAPI	4′,6-diamidino-2-phenylindole
EC	endothelial cell
EPO	erythropoietin
ERG	ETS-related gene
FACS	fluorescence-activated cell sorting
FB	fibroblast
GPRC5A	G-protein–coupled receptor class C group 5 member A
GLUT1	glucose transporter 1
HE	hematoxylin and eosin
HIF	hypoxia inducible factor
IB4	isolectin B4
KO	knockout
LV	left ventricle
LDHA	lactate dehydrogenase
LVEF	LV ejection fraction
LVED	LV end-diastolic
LVES	LV end-systolic
MoLUS	Mouse Lung UltraSound
NG2	neuron-glial antigen 2
O2	oxygen
PDPN	podoplanin
PC	pericyte
PGK	phosphoglycerate kinase
PH	pulmonary hypertension
PH3	phospho histone H3
PHD	prolyl-4-hydroxylase
Rai3	retinoic acid inducible protein 3
RV	right ventricle
RVSP	right ventricular systolic pressure
RVWT	RV wall thickness
SMA	smooth muscle actin
SMC	smooth muscle cell
SPC	surfactant protein C
TAPSE	tricuspid annular plane systolic excursion
VEGF	vascular endothelial growth factor
VHL	von Hippel-Lindau
VSMC	vascular smooth muscle cell
WGA	wheat germ agglutinin
Wt1	Wilms tumor 1

Highlights

- Vascular HIF2 (hypoxia inducible factor 2) promotes pulmonary vascular remodeling in response to chronic hypoxia, leading to elevated right ventricular systolic pressure.
- HIF2 is required for pulmonary microvascular stability upon low oxygen exposure and prevents alveolar swelling and lung congestion.
- Vascular HIF2 signaling protects from cardiomegaly, heart failure, excessive capillary proliferation, and remodeling during sustained hypoxia.
- The protective role of HIF2 preserving cardiac and pulmonary microvasculature is modulated by oxygen levels, and the cardiopulmonary defects induced by HIF2 deletion are rescued upon reoxygenation.

(glucose transporter 1), PGK (phosphoglycerate kinase), or LDHA (lactate dehydrogenase a), which function to metabolically adapt the tissue to oxygen deprivation and anaerobic ATP synthesis. HIF2 induces EPO (erythropoietin) and VEGF (vascular endothelial growth factor), which are important to improve oxygen supply to the hypoxic region.[5,6] Although HIF1 and HIF2 bind to an identical core-binding motif within the hypoxia response elements 5′-RCGTG-3′, they have unique targets not compensated by the complementary isoform. HIF1 contributes more to the acute hypoxia-driven transcriptional responses, like cellular glycolysis or adenosine release after injury, while HIF2 has been mostly related to chronic adaptation to hypoxia.[7] Both isoforms have been associated with several pathologies.

It is well established that HIFs play an important role in the heart homeostasis and along the progression of cardiovascular diseases.[8] During development, HIF1α is expressed in the embryonic heart,[9–12] where it governs a glycolytic metabolism of the compact myocardium.[11,12] In contrast, the role of HIF2 during heart development remains poorly understood. Global HIF2 deletion affects catecholamine production in the organ of Zuckerkandl, leading to prominent bradycardia and cardiac dysfunction.[13] Nevertheless, the phenotype of full HIF2 knockout mice varies depending on the genetic background.[13–15] In the lungs, HIF signaling has also been reported to execute important functions. HIF1α is implicated in bronchial epithelial formation, while HIF2 is mostly expressed in the vascular endothelium and alveolar type II cells, playing a crucial role in vascular morphogenesis and surfactant production during lung development.[16] In contrast to the limited knowledge about HIF2 function in the heart, the role of HIF2 signaling has been extensively studied during the development and progression of pulmonary hypertension (PH). PH is a cardiovascular disorder that can appear in patients with chronic obstructive pulmonary disease, after prolonged exposure to hypoxia or because of living at high altitude (World Health Organization class 3).[16] PH is characterized by significant vascular remodeling of the distal pulmonary arteries, resulting in reduced vascular lumen and increased resistance,

which leads to elevation of the right ventricular systolic pressure (RVSP) that eventually could lead to heart failure.[16] In this context, the role of HIF1 and HIF2 in endothelial cells (ECs) during the onset of PH has been extensively studied.[16–20] Several lines of evidences using *VE-CadherinCre* (*Cdh5*),[17] *Tie2Cre*,[18] or *L1Cre*[19] models to mediate endothelial-specific deletion of HIFs have uncovered the essential role of HIF2 in mediating pulmonary arterial remodeling associated to vasoconstriction, proliferation of ECs and vascular smooth muscle cells (VSMCs), as well as fibrosis, causing the occlusion of the pulmonary arteries and increasing the RVSP.[20] Recent publications have investigated the importance of HIF signaling during muscularization in mural cells, either VSMC[21,22] or pericytes (PCs),[23] reporting that they are not involved in the remodeling process as the ECs are. However, the role of HIF2 in non-ECs within the vascular compartment during the response to chronic hypoxia, especially in the heart, remains elusive. In that regard, the use of alternative genetic strategies able to simultaneously delete *Hif2α* in several vascular cells might be of interest to better understand the general function of HIF2 in PH, where the interaction between several cell types is necessary for disease progression. Furthermore, a broader inhibition within vascular cells may help to evaluate the potential impact of systemic administration of HIF2 inhibitors for disease treatment,[24,25] as HIF2, or any of its target genes, may have special or even opposite functions in different PH-involved cell types.

Despite the notion that PH is more prevalent in females than in males, with an estimated ratio of 4.3:1 for all forms of PH,[26] males with PH usually have a worse prognosis, which seems to be dependent on estrogen-associated cardiac and vascular protection or either to a better response of females to current treatments (revised in the study by Mair et al[27]). In addition, numerous studies performed in rats, either with monocrotaline or chronic hypoxia, also reported some sex effects on the appearance and progression of PH.[28] Nevertheless, our knowledge of the sex effect on the setting of mouse models of PH is still limited. Indeed, several investigations in mice proposed that estrogens might in fact enhance vascular remodeling by impacting on the proliferative capacity of pulmonary arterial smooth muscle cells (SMCs).[29] However, estrogens seem to play a cardioprotective role, as estrogen therapy can reverse advanced defects of PH like right ventricular (RV) maladaptive hypertrophy and RV dysfunction.[30,31]

Wt1 (Wilms tumor 1) is a transcription factor with a critical role in organogenesis and adult homoeostasis. During embryogenesis, Wt1 contributes to the mesothelium of most organs of the coelomic cavity, including the heart, lungs, spleen, liver, stomach, and the intestine, being also essential for proper development and homeostasis of the kidneys and the urogenital system.[32] During cardiogenesis, Wt1 contributes to epicardial progenitors that give rise to coronary vasculature and interstitial fibroblasts (FBs) through a process of epithelial-to-mesenchymal transition.[33–35] Furthermore, Wt1 is expressed in a small fraction of cardiomyocytes,[36,37] and it has been reported that Wt1 is also expressed in postnatal noncoronary ECs of the microvasculature.[38] In the lungs, Wt1 contributes to the pulmonary mesenchyme forming the vascular and bronchial SMCs, tracheal cartilage, and part of the arterial endothelium, as well as to fibroblast-like cells from the airways.[39] Nevertheless, the adult lineage tracing of Wt1 in the lungs has not been evaluated to the best of our knowledge.

The goal of our research was to evaluate the importance of HIF2 signaling in the development of coronary vasculature derived from Wt1 epicardial progenitors and to determine the role of HIF2 beyond the endothelium during the cardiac and pulmonary adaptation to low oxygen tensions. Our genetic strategy aims to evaluate possible side-effects of novel therapeutic approaches based on HIF2 inhibition,[24,25] as HIF2 plays important roles in several cell types contributed by the Wt1 lineage. For that purpose, here, we generated and characterized a novel mouse model of simultaneous HIF2 deletion in cardiopulmonary vascular and interstitial populations in homeostasis and in response to chronic hypoxia using the *Wt1Cre* line.[40] In contrast to former tools, this model allows us to evaluate the impact of concurrent elimination of HIF2 in ECs, PCs, SMCs, and FBs of the heart and lungs and hence, is a valuable genetic strategy to anticipate potential effects of systemic HIF2 abrogation. Our data reveal that HIF2 is not required for proper coronary vasculature development during cardiogenesis. Moreover, the lack of HIF2 signaling in the Wt1 lineage protects against the elevation of the RVSP during chronic hypoxia by preventing arteriolar muscularization, while it results in lung capillary leakage, alveolar hemorrhages, inflammation, and pulmonary congestion. Furthermore, elimination of HIF2 in the Wt1 compartment has detrimental effects on the cardiac adaptation to sustained low oxygen, leading to cardiomegaly, ventricular hypertrophy, dilatation, and systolic dysfunction, together with microvascular instability. Interestingly, most of these cardiopulmonary structural abnormalities are rescued after 1 week of reoxygenation, while cardiac function remains affected. Remarkably, we do not observe significant differences between male and female *Hif2/Wt1* cKO mice, suggesting that HIF2-mediated responses to low oxygen are sex independent. Our data uncover novel protective roles of HIF2 in the heart and lungs in response to chronic hypoxia beyond its negative effect on the arterial endothelium and suggest that cardiopulmonary HIF2 signaling exerts a positive function preventing excessive capillary remodeling in response to low oxygen. Our work expands our limited knowledge on the role of HIF2 in the cardiovascular system during sustained hypoxia and might be relevant in the setting of novel pharmacological strategies based on HIF2 inhibition for PH.[24,25]

MATERIALS AND METHODS

Data Availability

The authors declare that all the data supporting the in vivo characterization are available within the main text of the article or within the Supplemental Material. Detailed experimental procedures or data supporting the findings of this study are available from the corresponding author upon reasonable request. Material transfer agreements are required for the donation of mice.

Animal Models and Study Approval

The Hif2$^{flox/flox}$ (Epas1^{tm1Mcs}/J),[41] Rosa-tdTomato (B6.Cg-Gt(ROSA)26Sor$^{tm14(CAG-tdTomato)Hze}$/J), and Ng2-DsRed (Tg(Cspg4-DsRed.T1)1Akik/J)[42] mouse lines were obtained from The Jackson Laboratory and maintained in homozygosity. The Wt1Cre mouse line was kindly provided by Dr De La Pompa[40] and maintained in heterozygosity. All mouse lines were grown on a C57BL/6 background. Strain details are listed in the Major Resources Tables in the Supplemental Material. To generate the Hif2 floxed/Wt1Cre mouse line (*Hif2/Wt1* cKO [conditional knockout]), homozygous Hif2$^{flox/flox}$ females were crossed with heterozygous Wt1-Cre$^{+/-}$ to obtain Hif2$^{flox/flox}$/Wt1-Cre$^{+/-}$ (*Hif2/Wt1* cKO) and control Hif2$^{flox/flox}$/Wt1-Cre$^{+/+}$ littermates. Hif2$^{flox/flox}$/Wt1-Cre$^{+/-}$ mice were crossed with the Rosa-tdTomato mouse line to generate the conditional *Hif2/Wt1* reporter line. We did not find any difference on the phenotypic manifestations between *Hif2/Wt1* cKO males and females. Hence, both sexes were indistinctly used for all the experiments. Mice were housed in SPF (specific-pathogen-free) conditions at the Centro Nacional de Investigaciones Cardiovasculares (CNIC) Animal Facility. Welfare of animals used for experimental and other scientific purposes conformed to European Union (EU) Directive 2010/63EU and Recommendation 2007/526/EC, enforced in the Spanish law under Real Decreto 53/2013. Experiments with mice were allowed by the authorized Environmental Department of Comunidad de Madrid, Spain, and the CNIC Animal Experimentation Ethics Committee with reference number PROEX 267/19.

Genotyping

All mice were genotyped by polymerase chain reaction. Primer sequences and further genotyping details can be found in Methods in the Supplemental Material.

Hypoxia Exposure and Reoxygenation Protocol

Twelve-week-old mice (male and female) were placed for 2 or 3 weeks inside a hypoxia chamber from Coylab (O_2 Control Glove Box 1 Person Polymer, 220v). The hypoxia chamber was equipped with an oxygen (O_2) control system (programed at 10% O_2), a nitrogen gas regulator, and an animal filtration system. After hypoxia exposure, mice were immediately analyzed by cardiac or lung echography and later on euthanized following the accepted protocols to proceed with organ extraction for tissue analysis. For reoxygenation experiments, the cages with animals exposed to 2 or 3 weeks of hypoxia at 10% O_2 were placed in normal ambient condition for an additional week before echography analysis and organ collection.

Cardiopulmonary-Echography and Analysis

Transthoracic echocardiography was blindly performed by an expert operator with a 30-MHz probe (Vevo 2100; VisualSonics, Canada). Mice were slightly anesthetized with 1% to 2% isoflurane in 100% oxygen, adjusted to maintain podal reflex (≈400–500 bpm). To assess the RV, tricuspid annular plane systolic excursion (TAPSE), pulmonary artery acceleration time/ejection time ratio (AT/ET), and RV wall thickness (RVWT) were measured. An apical 4- chamber view was selected to obtain TAPSE, by M mode. Pulmonary flow was acquired from a parasternal short-axis view at the level of the great vessels, using pulsed-wave Doppler. An angle short-axis view to optimized RV wall visualization was obtained to measure the wall thickness by M mode. Additionally, standard short-axis view and parasternal long-axis view in B and M modes were recorded and left ventricular (LV) dimensions and function were analyzed. LV end-diastolic (LVED) and end-systolic (LVES) areas were traced for automatic calculation of the LV end-diastolic and end-systolic volumes, as well as the LV ejection fraction (LVEF). In addition, both sides of the lungs were longitudinally scanned. With these lateral views, we analyzed the pleural pattern, the line profile, and the predominant color indicative of edema to calculate the mouse lung ultrasound score (MoLUS). To assess the MoLUS, we assigned a value for each type of parameter (lung sliding [horizontal movement of the pleural], line profile [A or B], color profile [black or white], Z lines and pleural thickness, defects, and effusion), according to its severity as previously described.[43] The final score is the sum of all values for an individual. Images were analyzed offline by a second blind operator.

RVSP Measurement

Mice were anesthetized with medetomidine (1 mg/kg) and ketamine (75 mg/kg). RVSP was measured by closed-chest insertion of the Venofix A catheter (27G), coupled to a pressure transducer (Transpac IV), directly into the RV. Hemodynamic data were recorded using the Biopac MP36R System and the Biopac Acknowledge 4.1.0 software. For each mouse, at least 30 seconds of continuous and stable heartbeat cycles without noise were selected to obtain the average RVSP.

Heart and Lung Extraction and Processing

Mice were euthanized by CO_2 inhalation following the approved protocol. Whole-mount analysis to determine organ and body weight changes was performed at dissection. Samples were fixed for 1 hour (for endothelial markers) or overnight (for histological staining and non-endothelial markers) at 4 °C in 4% PFA (paraformaldehyde) or formalin 10%. After fixation, samples were embedded in 30% sucrose and frozen in OCT (optimal cutting temperature) medium for later cryosection (8 µm) preparation in a cryostat (CM1950; Leica) or were dehydrated and embedded in paraffin for sectioning at 4 µm in a microtome (RM2155; Leica). Reagent references are detailed in the Major Resources Tables in the Supplemental Material.

Histological and Immunohistochemical Analysis

Histological analysis of the heart and lungs was performed using 4-µm-thick paraffin sections. Sections were stained with hematoxylin and eosin (HE) for structural characterization. For arterial remodeling evaluation, lung sections were stained with an antibody against SMA (smooth muscle actin) following standard histological analysis at the CNIC Histopathology Facility. HE- and SMA-stained slides were scanned using the Hamamatsu NanoZoomer 2.0RS device, and the image analysis and measurements were performed using NDP view (Hamamatsu, Japan) and ZEN 31 Blue Edition Lite. For immunostaining of paraffin sections, the samples were rehydrated and antigens were retrieved by incubation in citrate buffer pH 6 (10 mmol/L sodium citrate) for 20 minutes in a microwave. Sections were permeabilized with PBST (phosphate-buffered saline with triton) 0.4% (PBS [phosphate-buffered saline] 1X+Triton TX100) for 15 minutes shaking and blocked with blocking solution (PBST 0.1% with 5% goat serum) during 1 hour in a dark humid chamber. For OCT sections, samples were placed at room temperature for 1 hour and washed with distillated water for another hour. Upon complete removal of OCT, the sections were permeabilized and blocked as for paraffin sections. After blocking, sections were incubated with primary antibodies in blocking solution overnight at 4 °C. After washing 3× with PBST 0.1%, sections were incubated with secondary antibodies and DAPI (4′,6-diamidino-2-phenylindole) in PBS 1X for 1 hour at room temperature in darkness and mounted in fluorescent mounting medium. Images were acquired with Leica SP8 Navigator, Leica gated STED-3X-WLL SP8, or Stellaris confocal microscopes. The references of primary and secondary antibodies and reagents used in this study are listed in the Major Resources Table in the Supplemental Material.

Quantification of Immunostaining

Immunofluorescence staining was quantified using ImageJ.[44]

Cell Lineage Labeling Strategy for Heart and Lung Populations by Flow Cytometry Analysis

Mice were euthanized and subsequently, the heart and all the lung lobes were perfused with HBSS (Hanks' Balanced Salt Solution) to clean the blood inside the tissues. On the one hand, the atria, valves, and the large vessels of the heart were removed with surgical scissors, leaving only the ventricles for further analysis. On the other hand, the bronchi and trachea of the lungs were removed, leaving only the lobes. Once the tissues had been processed, cardiac ventricles and lobes of the lungs were minced separately on iced PBS. Minced heart was digested with collagenase A (2.5 mg/mL), liberase (0.25 mg/mL), and DNase I (100 U/mL). Minced lungs were digested only with liberase (0.25 mg/mL) and DNase I (100 U/mL). Both tissues were digested during 30 minutes in a water bath at 37 °C with shaking every 5 minutes. Next, the digestion reaction was stopped by adding HBSS and the final single-cell suspensions were obtained by mechanical dissociation and filtering in 70 µm and subsequently in 40 µm Cell Strainer.

Before starting the cell lineage labeling, an erythrocyte lysis with red blood cells lysis buffer 1X (prepared from a 10× solution: 82.9 g/L ammonium chloride NH_4Cl, 10 g/L potassium bicarbonate $KHCO_3$, 2 mL/L EDTA [ethylenediamine tetra-acetic acid] 0.5 M, fill up to 1 L of distilled water pH 7.2–7.4) was performed for 15 minutes on ice. Red blood cells lysis reaction was stopped by adding Fluorescence-Activated Cell Sorting (FACS) buffer (PBS 1X; 2.5% inactive FBS [fetal bovine serum] and 0.5 M EDTA). Single-cell suspensions were incubated for 45 minutes in rotation at 4 °C with conjugated antibodies against CD (cluster of differentiation) CD45, CD90.2, CD31, PDPN (podoplanin)-Gp38 (Glycoprotein 38), and CD39 to define gates for nonmyocyte populations in the heart and lungs as previously described by others.[45–48] References, working dilutions, and vendors for flow cytometry studies are detailed in the Major Resources Table in the Supplemental Material. SYTOX Green was used as a viability marker. Samples were acquired in BD LSRFortessa SORP and BD FACSAria Fusion Cell Sorter (BSL-2 [Biosafety level 2]) equipped with the DIVA software. FlowJo was used to analyze the data.

Quantification of Nonmyocyte Cell Percentage or Total Number per Gram of Tissue

To calculate the percentage of nonmyocyte cells in the heart and lungs contributed by the Wt1 lineage, we used Wt1-Cre/Rosa-tdTomato and followed the digestion and

labeling strategy described above. To determine the contribution to each cardiac and lung lineage, we calculated the number of each cell population within the CD45⁻/Wt1-Tomato⁺ gate relative to the total Tomato⁺ cells following the formula

$$\frac{n\ cells\ of\ each\ population\ within\ Tomato+}{total\ Tomato+} \times 100$$

To determine the absolute number of each cell lineage contributed by Wt1 in different mice, we used beads to normalize the value per gram of tissue. In particular, we used Truecount beads (663028; BD Biosciences) that were prepared at 10 000 beads/mL of FACS buffer with SYTOX Green, viability marker. Of this beads buffer, 500 µL was added to the cell suspension (already labeled) described above. Approximately 1000 beads were acquired per sample. The quantification of the number of cells per gram of tissue was calculated with this formula:

$$\frac{cells}{beads} \times \frac{total\ Beads}{ml\ Beads\ buffer} \times \frac{ml\ Beads\ buffer\ used}{fraction\ of\ single-cell\ solution\ used} \times \frac{n\ samples}{weight\ of\ tissue\ (mg)} = \frac{cell}{mg}$$

In this equation, cells/beads are the exact number of cells/beads after FlowJo analysis. Total beads/mL beads buffer are 10 000 beads/1 mL beads buffer. Of the beads buffer, 0.5 mL was used per 0.1 mL of single-cell suspension of digestion tissue, and per tube, there was only 1 sample.

Statistical Analysis and Study Design

Statistical analyses were performed using the GraphPad Prism 10 software. All results are presented as mean±SEM. Normal distribution of the data was tested by using the Shapiro-Wilk test (α [significance level] =0.05) for small samples and Kolmogorov-Smirnov test (α=0.05) for large samples. In case of normal distribution, the unpaired 2-tailed Student *t* test was used (α=0.05; CI [confidence interval] of 95%). For comparison of multiple groups (>2 groups), a 1-way ANOVA followed by a Tukey post hoc test was used. $P<0.05$ was considered to be statistically significant. Nonsignificant results ($P>0.05$) were not shown in the graphs.

Samples were analyzed blinded by different researches, and groups (control and *Hif2/Wt1 cKO* mutant mice) were randomly assigned to each condition (normoxia, 2 weeks of hypoxia, 3 weeks of hypoxia, and reoxygenation). No prior statistical group size determination was performed. Instead, group size was determined according to previous experience and reproducibility of the results across the independent experiments. No animals were excluded from the study unless due to ethic end points criteria associated with the treatment or genotype. Images were chosen according to the most representative examples reflecting the typical phenotype.

RESULTS

Wt1 Lineage Contributes to the Macrovascular and Microvascular Compartments of the Heart and Lungs

To further investigate Wt1 lineage in the adult heart, we performed lineage tracing analysis using a Rosa-tdTomato reporter mouse. We confirmed the previously reported contribution of Wt1 lineage to coronary arteries[35,49] including ECs (ERG [ETS-related gene]⁺) and VSMCs (SMA⁺;Figure 1A). Additionally, we identified that Wt1 lineage also contributes to PCs (CSPG [chondroitin sulfate proteoglycan 4] or NG2 [neuron-glial antigen 2])⁺ and interstitial FBs (PDPN [or GP38]⁺) surrounding and connecting the capillaries of the microvasculature (Figure 1B). We further investigated Wt1 lineage contribution to major cardiac cell populations by flow cytometry using the Rosa-tdTomato/Wt1Cre mice. FACS analysis showed that Wt1 lineage contributed to 31.4% of CD45⁻ nonmyocyte cells in the adult heart (Figure 1C). Within the Tomato⁺-Wt1-derived cells, around 6.4% corresponds to CD39⁺/CD90⁺ VSMCs (Figure 1D), 24% to CD90⁺/GP38⁻ PCs (Figure 1E), 50.1% to CD31⁺ ECs (Figure 1F), and 8.4% to CD31⁻/CD90⁻/GP38⁺ FBs (Figure 1F; Table S1). Furthermore, we calculated the relative contribution of Wt1 lineage within each nonmyocyte population and determined that there is a significant percentage of cardiac vascular cells contributed by the Wt1 lineage, especially PCs, SMCs, and FBs that are contributed 81.3%, 73.3%, and 56.4%, respectively, by the Wt1 lineage in the heart (Table S2). Therefore, despite the fact that the endothelium is the main cell type within the Wt1 lineage, ECs derived from the Wt1 lineage only represent around 23% of cardiac ECs (Table S2).

Regarding the adult lungs, using the same reporter model of Rosa-tdTomato/Wt1Cre, we found that Wt1 lineage contributes to ECs of the alveolar capillary network, small and large arteries, as well as to SMCs in the medial layer of pulmonary arteries and in the bronchial submucosa (Figure 1G). Wt1 lineage also contributes to parenchymal PCs (Figure 1H). In contrast, there is no contribution to alveolar type I or type II cells identified by Rai3 (retinoic acid inducible protein 3), also known as GPRC5A (G-protein–coupled receptor class C group 5 member A)[50] or SPC (surfactant protein C[48,51]; Figure S1A), or to alveolar macrophages labeled by IB4 (isolectin B4[52]; Figure 1I). As in the heart, we further investigated Wt1 lineage contribution to major lung cell populations by flow cytometry using Rosa-tdTomato/Wt1Cre mice. FACS analysis showed that over 18.3% of the CD45⁻ fraction of adult lungs expresses or is Wt1- derived (Figure 1J). Of these Tomato⁺ cells, around 37.3% corresponds to CD31⁺/CD39⁺ endothelium (Figure 1K), 20.6% to CD31⁻/CD39⁺ SMCs (Figure 1K), 22.8% to

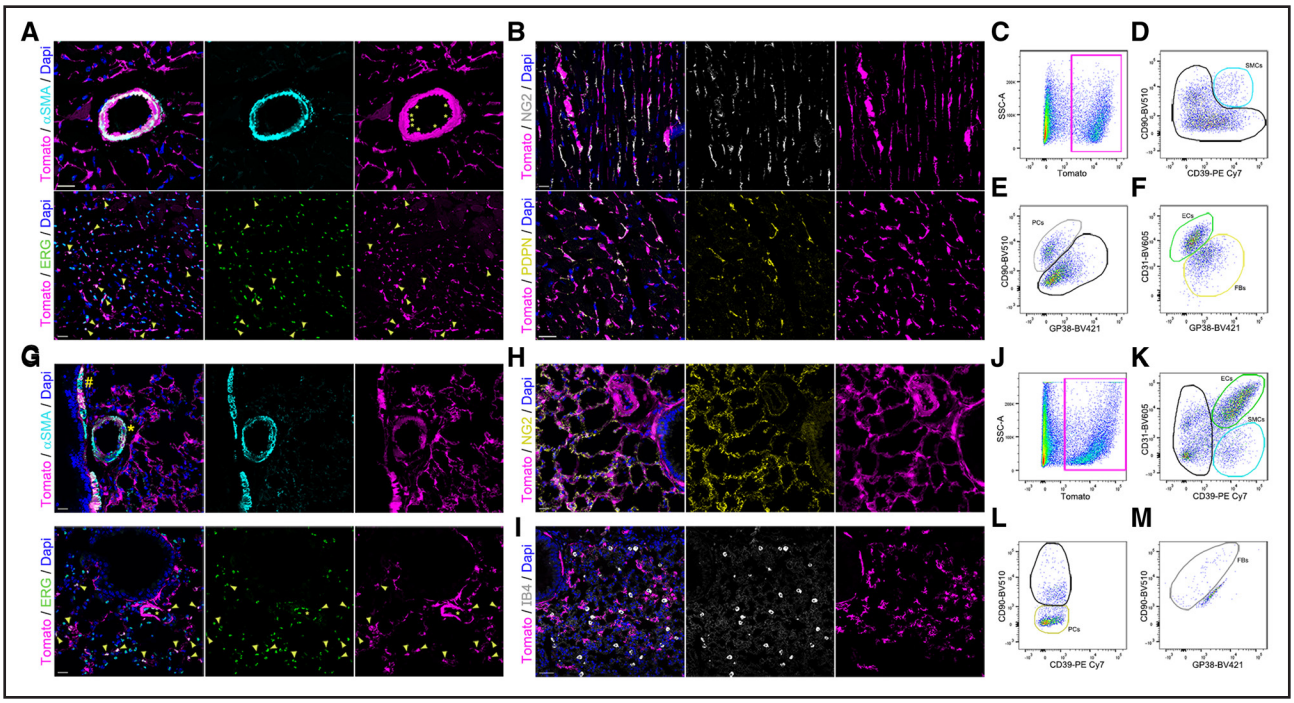

Figure 1. Wt1 (Wilms tumor 1) lineage contribution to the heart and lungs.
A and **B**, Immunofluorescence of cardiac sections from Rosa-tdTomato/Wt1Cre reporter mice with cell lineage markers. **A**, αSMA (α-smooth muscle actin; vascular smooth muscle cells [VSMCs], cyan), ERG (ETS-related gene; endothelial cells [ECs], green), DAPI (4′,6-diamidino-2-phenylindole; nucleus, blue), and Tomato (Wt1 lineage, magenta). **Top**, Complete colocalization of αSMA$^+$/Tomato$^+$ signal and some ECs (yellow asterisks) in a coronary artery. **Bottom**, ERG$^+$/Tomato$^+$ ECs of capillaries (yellow arrowheads). Scale bars=20 µm. **B**, **Top**, Colocalization between NG2 (neuron-glial antigen 2; pericytes [PCs], white) and Tomato (Wt1 lineage, magenta). **Bottom** portions are stained with PDPN (podoplanin; fibroblasts [FBs], yellow) and Tomato (Wt1 lineage, magenta). Nuclei are costained with DAPI (blue). Scale bars=20 µm. **C** through **F**, Representative flow cytometry plots for identification of nonmyocyte cardiac populations within the Wt1 lineage. **C**, Magenta rectangle contains Tomato$^+$ cells within all CD (cluster of differentiation) 45$^-$ cells. **D**, Within Tomato$^+$ cells in **C**, the cyan gate contains CD90$^+$/CD39$^+$ SMCs. **E**, From the black gate on **D**, the gray gate corresponds to CD90$^+$/GP (glycoprotein) 38$^-$ PCs. **F**, From PC$^-$ in **E**, the green gate represents CD31$^+$/GP38$^-$ ECs and the yellow gate represents CD31$^-$/GP38$^+$ FBs. **G** through **I**, Immunofluorescence of lung sections of Rosa-tdTomato/Wt1Cre reporter mice with cell lineage markers. **G**, αSMA (VSMCs, cyan), ERG (ECs, green), DAPI (nucleus, blue), and Tomato (Wt1 lineage, magenta). **Top**, Colocalization of αSMA$^+$/Tomato$^+$ in the bronchial submucosa (yellow hash) and in the medial layer of a pulmonary artery (yellow asterisk). **Bottom**, Alveolar ERG$^+$/Tomato$^+$ ECs (yellow arrowheads). Scale bars=20 µm. **H** and **I**, Colocalization of Tomato (Wt1 lineage, magenta) with NG2 (**H**, PCs, yellow) but not with IB4 (isolectin B4; **I**, alveolar macrophages, white). Nuclei are costained with DAPI (blue). Scale bars=20 µm (**H**) and 40 µm (**I**). **J** through **M**, Representative plots of the flow cytometry strategy to characterize Wt1 pulmonary lineage. **J**, Magenta rectangle contains positive selection of Tomato$^+$ cells within all CD45$^-$ cells. **K**, Within Tomato$^+$ cells, the cyan gate represents CD90$^+$/CD31$^-$ SMCs and the green gate, CD31$^+$/CD39$^+$ ECs. **L**, From the SMC/EC black gate in **K**, PCs were identified as CD39$^-$/CD90$^-$. **M**, Finally, we excluded cell autofluorescence detected with the single markers (data not shown) and kept the CD90$^+$/GP38$^-$ as the FB gate (gray). BV421 indicates brilliant violet 421; BV510, brilliant violet 510; PE-Cy7, phycoerythrin cyanine 7; and SSC-A, side scatter-area.

CD90$^-$/GP38$^-$ PCs (Figure 1L), as further confirmed by NG2-DsRed reporter mice (Figure S1B), and 1.7% to CD90$^+$ FBs (Figure 1L and 1M; Table S3). As in the heart, despite the higher proportion of ECs contributed by the pulmonary Wt1 lineage (37.3%) compared with other cell types, these ECs just represent 20.65% of the lung endothelium (Table S4). The relative contribution of Wt1-derived cells to other pulmonary lineages was also determined (Table S4).

In summary, these lineage tracing analyses demonstrated that Wt1 lineage contributes to macrovasculature and microvasculature of the heart and lungs, offering an important tool for genetic manipulation and molecular analysis of the different cell components involved in vascular function.

Elimination of HIF2 in the Wt1 Lineage Prevents Pulmonary Arteriole Muscularization and Protects Against Elevation of the RVSP Upon Chronic Hypoxia

To understand the role of HIF2 in the cardiovascular and pulmonary compartments contributed by Wt1 (Figure 1), we generated a new conditional HIF2 knockout model by crossing the *Hif2*-floxed[41] line with the *Wt1Cre* mouse line,[40] from now on *Hif2/Wt1* cKO. First, we confirmed efficient deletion of *Hif2*-floxed exon 2 by polymerase chain reaction (data not shown). Next, we determined that elimination of *Hif2* in the Wt1 lineage does not cause embryonic lethality or any obvious cardiovascular structural defect, including the proper formation of the

ventricular chambers or the coronary tree (Figure S2A). Furthermore, we confirmed that *Hif2/Wt1* cKO mice display normal survival curve from weaning to adulthood (Figure S2B), suggesting that Wt1/HIF2 signaling is not required for the correct formation and homeostasis of the heart. Afterward, we evaluated lung tissue integrity under normoxic conditions on whole-mount analysis (data not shown) and by HE staining of the lung parenchyma (Figure 2A), finding no obvious differences between the structure of control and *Hif2/Wt1* cKO mice in basal conditions. Thereafter, we investigated the impact of *Hif2* deletion in the Wt1 lineage in response to chronic hypoxia. To that aim, we exposed 12-week-old control and *Hif2/Wt1* cKO mice to 10% oxygen (O_2) during 2 or 3 weeks and evaluated the functional and structural parameters by echography and classical histology (Figure S3). Because it has been previously reported that hypoxia induces vascular remodeling by muscularization of distal pulmonary arterioles,[21,53] first we performed an SMA staining in lung sections in normoxia or after exposure to hypoxia (Figure 2B). Tissue analysis revealed that after 2 and 3 weeks of hypoxia, there were no significant differences between control and mutant mice on the number of large (30–20 µm; Figure 2C) or on medium (19–10 µm) caliber arterioles (Figure 2D), although there was an upward tendency in the number of medium arterioles of control mice with respect to *Hif2/Wt1* cKO mice. In contrast, this difference became highly significant for the number of small arteries (9–1 µm) found in control mice after 2 and 3 weeks of hypoxia compared with normoxic conditions, while *Hif2/Wt1* cKO mice exhibited a similar number of small arteries in both conditions (Figure 2E). Then, we determined the effect of the vascular remodeling differences after hypoxia exposure in the measurement of the RVSP. As expected, control mice displayed a significant elevation of the RVSP after 2 and 3 weeks of chronic hypoxia. In contrast, the *Hif2/Wt1* cKO mice were protected against the elevation of

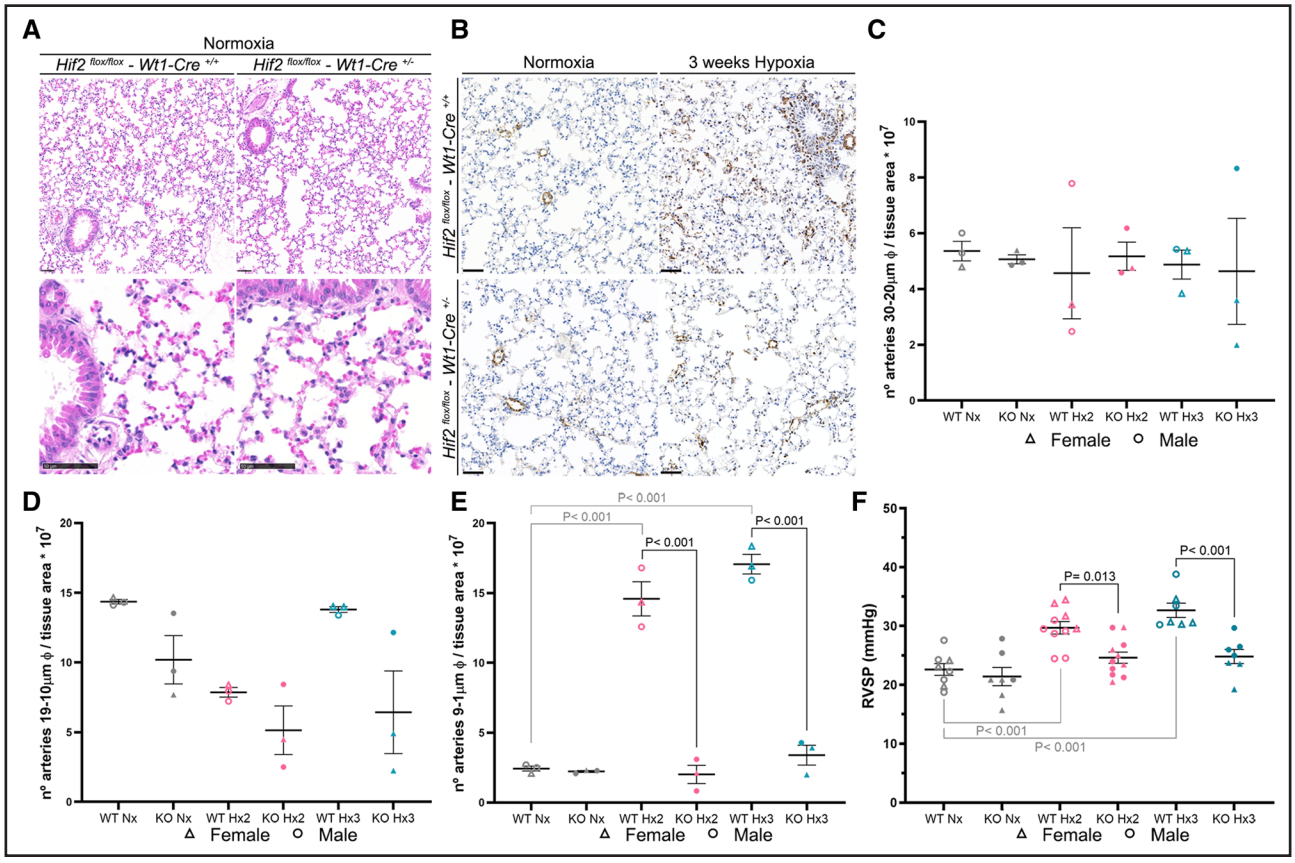

Figure 2. Muscularization of pulmonary arteries under chronic hypoxia.
A, Histological analysis by hematoxylin and eosin (HE) staining of lung sections from control ($Hif2^{flox/flox}$-$Wt1\text{-}Cre^{+/+}$, **left**) and *Hif2/Wt1* cKO (conditional knockout) mice ($Hif2^{flox/flox}$-$Wt1\text{-}Cre^{+/-}$, **right**) in normoxic conditions. Scale bars=50 µm. **B**, Representative images of αSMA (α-smooth muscle actin) immunohistochemistry in control ($Hif2^{flox/flox}$-$Wt1\text{-}Cre^{+/+}$, **top**) and *Hif2/Wt1* cKO mice ($Hif2^{flox/flox}$-$Wt1\text{-}Cre^{+/-}$, **bottom**) in normoxia (Nx) or chronic (3 weeks) hypoxia. Scale bar, 50 µm. **C** through **E**, Quantification of the number of lung arterioles ranging from 30 to 20 µm (**C**), 19 to 10 µm (**D**), or 9 to 1 µm (**E**) per tissue area in control (WT [wild-type]) and *Hif2/Wt1* cKO (KO [knockout]) mice in Nx (gray), after 2 weeks of sustained hypoxia (Hx2; pink), and after 3 weeks of sustained hypoxia (Hx3; blue). **F**, Scatter dot plot of the right ventricular systolic pressure (RVSP). All graph bars show individual values for females (triangles) and males (circles), and the black line represents the mean±SEM. The total distribution of sex was as follows: n=8 females and n=9 males (**C** through **E**) and n=23 females and n=27 males (**F**). Statistical significance was determined using a 1-way ANOVA multiple comparisons test with Tukey correction. Significant *P* values >0.001 are explicitly indicated, while *P* values <0.001 state as *P*<0.001. Nonsignificant (*P*>0.05) *P* values are not shown.

RVSP at both time points, showing similar pressures in normoxia or hypoxia conditions (Figure 2F). These results are in agreement with former works describing the role of endothelial HIF2 in arterial remodeling upon chronic hypoxia.[17–19]

Altogether, these data indicate that elimination of HIF2 in the Wt1 lineage prevents vascular remodeling and subsequent RVSP elevation after chronic hypoxia, protecting against hallmarks of PH in response to low oxygen.

Functional HIF2 in the Microvascular Compartment Is Necessary for Alveolar Parenchyma Stability and Pulmonary Performance During Sustained Hypoxia

To further investigate the importance of HIF2 signaling in the pulmonary Wt1 lineage, we performed lung and right-sided cardiac echography analysis in control and *Hif2/Wt1* cKO mice in normoxia and after 2 or 3 weeks of chronic hypoxia at 10% O_2. First, we determined the value of the pulmonary artery acceleration time/ejection time ratio (AT/ET) indicative of the pulmonary artery pressure, finding no significant differences between control and *Hif2/Wt1* cKO mice, neither in normoxia nor after 2 or 3 weeks of hypoxia (Figure 3A). Next, we calculated the mouse lung ultrasound score (MoLUS) that predicts the level of pulmonary congestion integrating several functional and structural parameters of the lungs (pleural effusion; alveolar edema/hemorrhages; and the presence or absence of A, B, and Z lines among others), and that has been previously reported to correlate with cardiac function.[43] Echographic analysis confirmed similar mouse lung ultrasound values between control and *Hif2/Wt1* cKO mice in normoxia and after 2 weeks of hypoxia exposure, but a notable increase on this parameter in HIF2 mutants after 3 weeks of sustained hypoxia (Figure 3B and 3C). These results indicated that, despite their protection against vascular remodeling (Figure 2C) and RVSP elevation (Figure 2G), *Hif2/Wt1* cKO mice displayed worse pulmonary performance and profound structural abnormalities during sustained hypoxia. To further investigate the extent of lung congestion in *Hif2/Wt1* cKO mice upon hypoxia, we analyzed the structure of the pulmonary parenchyma by HE staining, observing an important thickening of the alveolar wall in the *Hif2/Wt1* cKO mice relative to controls by 2 weeks of hypoxia (Figure 3D). Moreover, by 3 weeks of hypoxia, the *Hif2/Wt1* cKO mice lungs displayed severe erythrocyte congestion in the alveolar parenchyma, arterioles, and arteries (Figure 3D). This increased alveolar wall thickening and hemorrhages resulted in a significant reduction of the alveolar space in *Hif2/Wt1* cKO mice compared with controls after both 2 and 3 weeks of hypoxia exposure (Figure 3E). In addition, after 3 weeks of chronic hypoxia, there was an increased number of alveolar macrophages, many of them loaded with erythrocytes as evidenced by positive hemosiderin signal on HE staining (Figure 3F). We further confirmed the increase in the number of alveolar macrophages in the *Hif2/Wt1* cKO mouse lungs by 3 weeks of hypoxia by immunofluorescence with IB4 (Figure 3G and 3H), and its expansion with the proliferation marker Ki67 (Figure 3G and 3I). Since Wt1 lineage contributes neither to alveolar macrophages (Figure 1I) nor to alveolar type I or alveolar type II cells (Figure S1A), our results suggest that these alveolar alterations in the *Hif2/Wt1* cKO mice might be indirect and secondary to the abnormal vascular remodeling occurring in HIF2 mutants in response to sustained hypoxia. To evaluate this hypothesis, we analyzed whether the endothelium of the alveolar parenchyma was affected in the *Hif2/Wt1* cKO mice. Immunostaining with markers for ECs (ERG) and proliferation (Ki67) after exposure to chronic hypoxia (Figure 3G) showed a significant increase in the number of proliferating ECs in the *Hif2/Wt1* cKO mice compared with controls (Figure 3J).

Finally, FACS analysis from the lung tissue of Rosa-tdTomato/Wt1Cre reporter control or HIF2-floxed Rosa-tdTomato/Wt1Cre (*Hif2/Wt1* reporter cKO) mice revealed a significant elevation in total cells contributed by the Wt1 lineage (Tomato$^+$) in *Hif2/Wt1* reporter cKO compared with reporter control mice after 2 weeks of 10% O_2 exposure or with *Hif2/Wt1* reporter cKO mice in normoxia (Figure 4A). These quantitative changes by FACS analysis were further confirmed qualitatively by immunofluorescence (Figure 4B). The increase in total Tomato$^+$ cells could be explained by the elevation on Tomato$^+$ ECs in the *Hif2/Wt1* reporter cKO mice in hypoxia relative to normoxia and compared with reporter control mice after 2 weeks of hypoxia (Figure 4C and 4E). No significant changes were observed between control or *Hif2/Wt1* reporter cKO Tomato$^-$ ECs (Figure 4C and 4D). We observed no significant changes in the total Tomato$^+$ PCs in the lungs between normoxia or hypoxia in reporter control or in *Hif2/Wt1* reporter cKO mice, although there is a trend of induction in Tomato$^+$ PCs in the *Hif2/Wt1* reporter cKO compared with control mice after 2 weeks of chronic hypoxia (Figure 4F and 4H). In contrast, there is a reduction of Tomato$^-$ PCs from normoxia to hypoxia in the reporter control but not in the *Hif2/Wt1* reporter cKO mice (Figure 4G).

In summary, these results reveal that despite the protective effect on preventing pulmonary arteriole remodeling and elevation of RVSP, defective HIF2 signaling in the Wt1 compartment is deleterious for lung adaptation to chronic hypoxia. Indeed, HIF2 deletion in the Wt1 lineage results in unstable and proliferative microvasculature that favors erythrocyte extravasation and macrophage proliferation, leading to alveolar wall thickening, severe lung congestion, and pulmonary damage in response to chronic hypoxia.

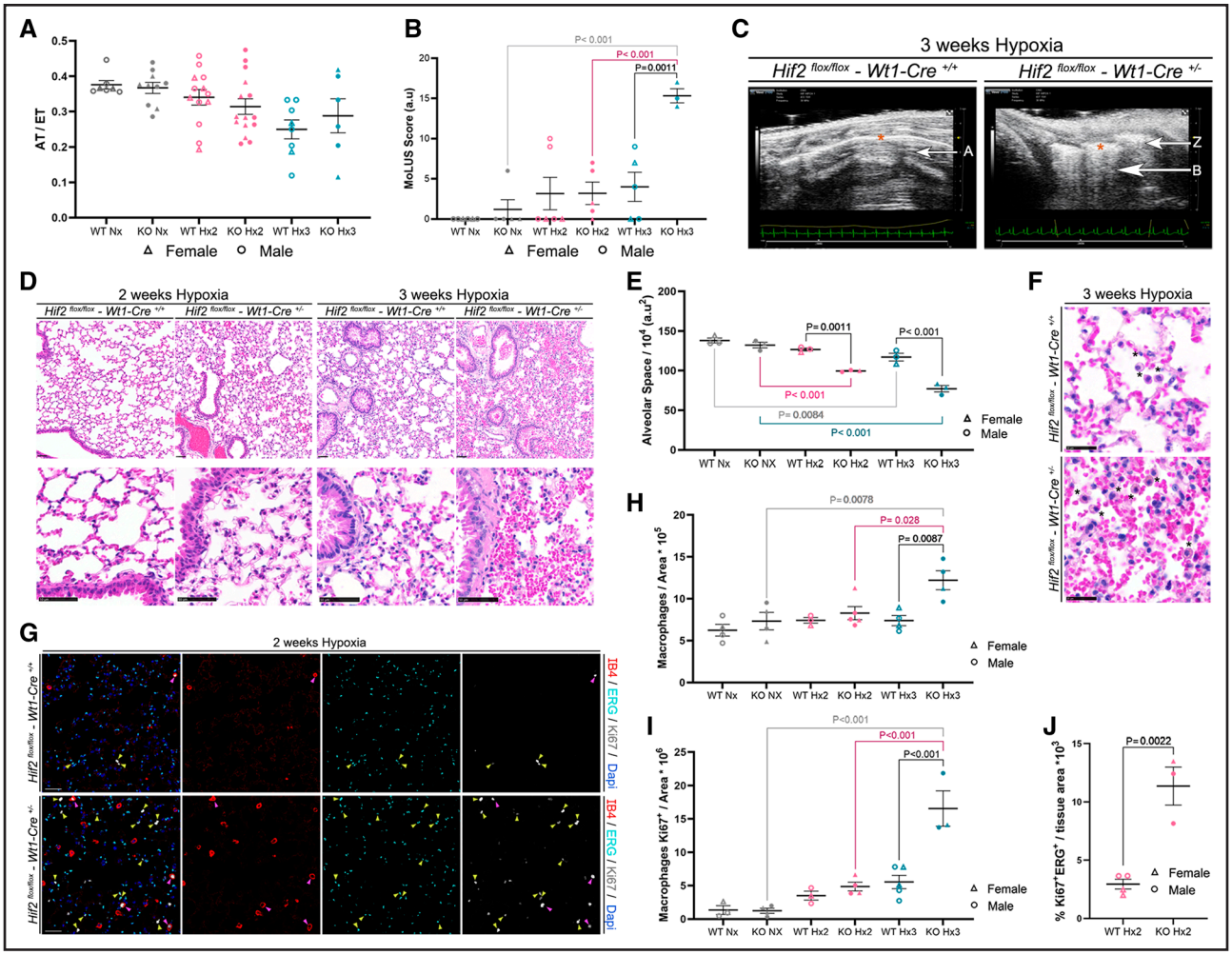

Figure 3. Pulmonary architecture and function during sustained low oxygen conditions.

A, Scatter dot plot of pulmonary artery acceleration time/ejection time ratio (AT/ET) measured by Doppler echography in control (WT [wildtype]) and *Hif2/Wt1* cKO (conditional knockout) (KO [knockout]) mice in normoxia (Nx; gray), 2 weeks of hypoxia (Hx2; pink), or 3 weeks of hypoxia (Hx3; blue). **B**, Scatter dot plot of mouse lung ultrasound score (MoLUS) of control (WT) and *Hif2/Wt1* cKO (KO) mice in Nx (gray) and hypoxia conditions (Hx2 [pink] or Hx3 [blue]). **C**, Representative lung echography images of control (Hif2$^{flox/flox}$-Wt1-Cre$^{+/+}$, **left**) and *Hif2/Wt1* cKO (Hif2$^{flox/flox}$-Wt1-Cre$^{+/-}$, **right**) mice after Hx3 exposure. B lines (white large tracks from top to bottom) and Z lines (white short lines under the pleura) reflecting pulmonary edema are obvious in the *Hif2/Wt1* cKO mice compared with controls with only A lines (fine lines parallel to the pleural line). Pleural thickening and fragmentation are evident in *Hif2/Wt1* cKO mice (white intense line, orange asterisk on **right**) compared with normal pleura indicative of well-aerated lungs (white thin line, orange asterisk on **left**). **D**, Histopathologic characterization by hematoxylin and eosin (HE) staining of lung sections of control (Hif2$^{flox/flox}$-Wt1-Cre$^{+/+}$, **left** of each condition of hypoxia) and *Hif2/Wt1* cKO mice (Hif2$^{flox/flox}$-Wt1-Cre$^{+/-}$, **right** of each condition of hypoxia). Scale bars=50 µm. **E**, Scatter dot plot showing the quantification of the alveolar space in control (WT) and *Hif2/Wt1* cKO (KO) mice in Nx (gray) and hypoxic conditions (Hx2 [pink] or Hx3 [blue]). **F**, Representative HE images of pulmonary inflammation showing alveolar macrophages (black asterisks) in control (Hif2$^{flox/flox}$-Wt1-Cre$^{+/+}$, **top**) and *Hif2/Wt1* cKO mice (Hif2$^{flox/flox}$-Wt1-Cre$^{+/-}$, **bottom**) after Hx3. Scale bars=25 µm. **G**, Representative immunofluorescence of pulmonary sections from control (Hif2$^{flox/flox}$-Wt1-Cre$^{+/+}$, **top**) and *Hif2/Wt1* cKO mice (Hif2$^{flox/flox}$-Wt1-Cre$^{+/-}$, **bottom**) stained for ERG (ETS-related gene; endothelial cells [ECs], cyan), Ki67 (mitosis, white), IB4 (isolectin B4; alveolar macrophages, red), and DAPI (4′,6-diamidino-2-phenylindole; nucleus, blue) showing proliferation of ECs (ERG$^+$/Ki67$^+$, yellow arrowheads) and alveolar macrophages (IB4$^+$/Ki67$^+$, pink arrowheads) after Hx2. Scale bars=20 µm. **H**, Scatter dot plot showing the quantification of macrophages per tissue area in controls (WT) and *Hif2/Wt1* cKO (KO) mice in Nx (gray) and hypoxic conditions (Hx2 [pink] or Hx3 [blue]). **I**, Number of proliferating macrophages per tissue area in lung sections from control (WT) and *Hif2/Wt1* cKO (KO) mice in Nx (gray) and hypoxia conditions (Hx2 [pink] or Hx3 [blue]). **J**, Percentage of EC proliferation (ERG$^+$/Ki67$^+$) per tissue area in control (WT) and *Hif2/Wt1* cKO (KO) mice after Hx2 exposure. All graph bars show individual values for females (triangles) and males (circles), and the black line represents the mean±SEM. The total distribution of mice sex was as follows: (**A**) n=20 females and n=37 males, (**B**) n=12 females and n=18 males, (**E**) n=7 females and n=11 males, (**H**) n=9 females and n=15 males, (**I**) n=9 females and n=13 males, and (**J**) n=3 females and n=4 males. Statistical significance was determined using a 1-way ANOVA multiple comparisons test with Tukey correction for **A**, **B**, **E**, **H**, and **I** and 2-tailed Student *t* test for **J**. Significant *P* values >0.001 are explicitly indicated, while *P* values <0.001 state as *P*<0.001. Nonsignificant (*P*>0.05) *P* values are not shown.

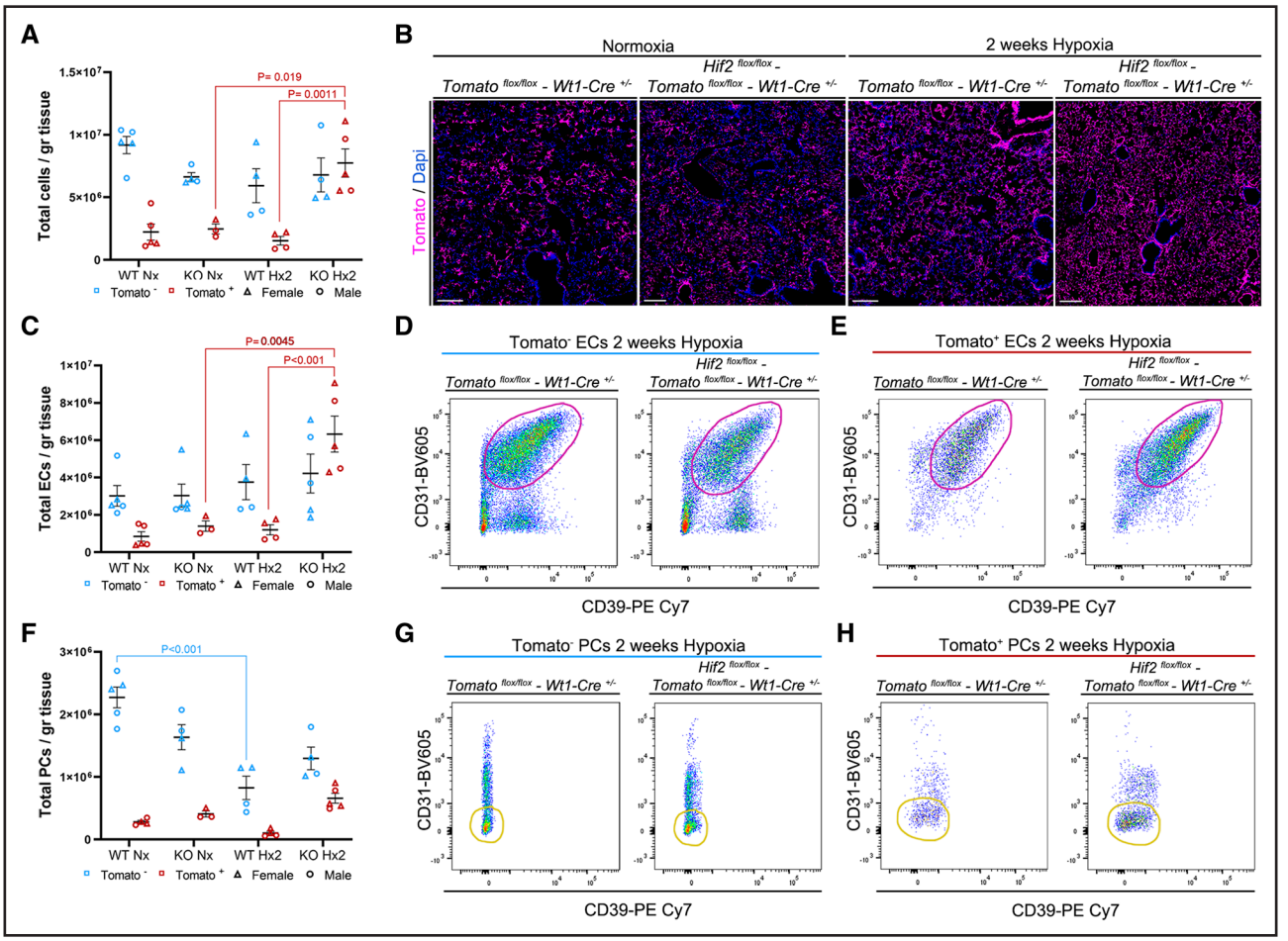

Figure 4. Quantitative analysis of Wt1 (Wilms tumor 1)-derived pulmonary cells during chronic hypoxia.
A, Quantification of total cells per gram of tissue of Tomato$^-$ (blue) and Tomato$^+$ (red) cells in Rosa-tdTomato/Wt1 reporter control (WT [wild type]) and Rosa-tdTomato/Hif2 reporter cKO (conditional knockout) (KO [knockout]) mice in normoxia (Nx) and after 2 weeks of hypoxia (Hx2) analyzed by FACS (Fluorescence-Activated Cell Sorting). **B**, Immunofluorescence of Tomato (Wt1 lineage, magenta) and DAPI (4′,6-diamidino-2-phenylindole; nucleus, blue) in lung sections from Rosa-tdTomato/Wt1 reporter control (Tomato$^{flox/flox}$-Wt1$^{+/-}$, **left** panel of each experimental condition) and Rosa-tdTomato/Hif2 reporter cKO mice (Tomato$^{flox/flox}$/Hif2$^{flox/flox}$/Wt1$^{+/-}$, **right** panel of each experimental condition) in Nx (left columns) and after Hx2 (right columns). Scale bars=200 µm. **C** and **F**, Scatter dot plots representing changes in the total cells per gram of tissue of Tomato$^-$ (blue) and Tomato$^+$ (red) endothelial cells (ECs; **C**) or pericytes (PCs; **F**) in control (WT) and mutant (KO) mice in Nx and after Hx2. **D**, **E**, **G**, and **H**, Representative FACS pseudocolor image showing Tomato$^-$ ECs (purple gates, **D**) and Tomato$^+$ ECs (purple gates, **E**) or Tomato$^-$-PCs (yellow gates, **G**) and Tomato$^+$-PCs (yellow gates, **H**) from control (Tomato$^{flox/flox}$-Wt1$^{+/-}$) and HIF2 mutant (Tomato$^{flox/flox}$-Hif2$^{flox/flox}$-Wt1$^{+/-}$) lung tissue. All portions show the EC and PC content from a fixed number of 24 000 CD (cluster of differentiation) 45$^-$ cells. For all scatter plots, individual values for females (triangles) and males (circles) are shown, and the black line represents the mean±SEM. The total distribution of mice sex was as follows: **A**, **C**, and **F**) n=16 females and n=18 males. Statistical significance was determined using a 1-way ANOVA multiple comparisons test with Tukey correction. Significant *P* values >0.001 are explicitly indicated, while *P* values <0.001 state as *P*<0.001. Nonsignificant (*P*>0.05) *P* values are not shown. BV605 indicates brilliant violet 605; and PE Cy7, phycoerythrin cyanine 7.

Hif2/Wt1 cKO Mutants Display Cardiac Hypertrophy and Ventricular Dilatation in Response to Low Oxygen Exposure

Because the Wt1 lineage has a broad contribution to several vascular compartments of the heart (Figure 1A and 1B), and considering that the direct role of HIF2 in cardiac function and tissue structure in response to chronic hypoxia remains elusive, we decided to explore the impact of *Hif2* abrogation in the Wt1 cardiac lineage upon sustained low oxygen exposure. To this aim, we exposed 12-week-old control and *Hif2/Wt1* mutant mice to 10% O_2 during 2 and 3 weeks (Figure S3) and performed cardiac functional and structural analysis before and after hypoxia treatment. Echocardiography characterization revealed that the lack of HIF2 in the Wt1 lineage favors cardiac hypertrophy of both the RV, and specially the LV, in response to low oxygen tensions, while controls remained unaltered (Figure 5A and 5B). Whereas RV systolic function (TAPSE [tricuspid annular plane systolic excursion]) was unaffected in mutant mice relative to controls after exposure to chronic hypoxia (Figure 5C), *Hif2/Wt1* cKO mice displayed common hallmarks of LV systolic heart failure, with a significant reduced LV ejection

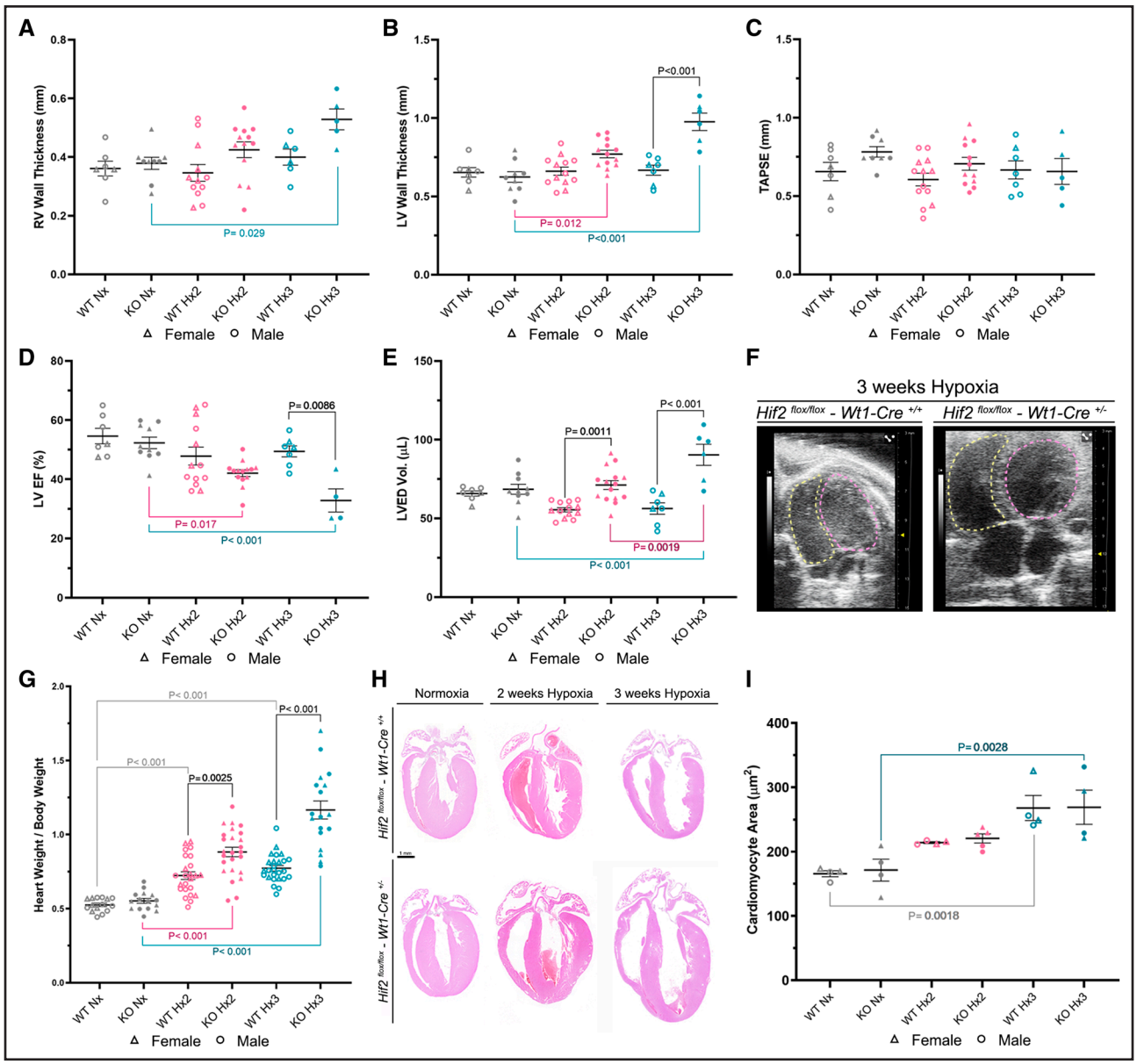

Figure 5. Cardiac functional and structural characterization in chronic hypoxia.
A through **E**, Functional analysis of the heart by echocardiography of control (WT [wild type]) and *Hif2/Wt1* cKO (conditional knockout) (KO [knockout]) mice in normoxia (Nx; gray), 2 weeks of hypoxia (Hx2; pink) or 3 weeks of hypoxia (Hx3; blue). **A**, Right ventricular (RV) wall thickness. **B**, Left ventricular (LV) wall thickness. **C**, Tricuspid annular plane systolic excursion (TAPSE). **D**, Left ventricular ejection fraction (LVEF). **E**, Left ventricular end-diastolic volume (LVED Vol). **F**, Representative images of a 2D view showing the apical 4-chamber view in control ($Hif2^{flox/flox}$-Wt1-$Cre^{+/+}$, **left**) and *Hif2/Wt1* cKO mice ($Hif2^{flox/flox}$-Wt1-$Cre^{+/-}$, **right**) after Hx3. The yellow dashed line delimits the inner face of the RV, while the pink dashed line defines the inner face of the LV. **G**, Quantification of the heart weight/body weight ratio in control (WT) and *Hif2/Wt1* cKO (KO) mice in Nx (gray) and Hx2 (pink) or Hx3 (blue). **H**, Representative histological analysis by hematoxylin and eosin (HE) staining of heart sections from control ($Hif2^{flox/flox}$-Wt1-$Cre^{+/+}$, **top**) and *Hif2/Wt1* cKO mice ($Hif2^{flox/flox}$-Wt1-$Cre^{+/-}$, **bottom**) mice in Nx (**left**), Hx2 (**middle**), or Hx3 (**right**). Scale bar=1 mm. **I**, Quantification of the cardiomyocyte area in controls (WT) and *Hif2/Wt1* cKO (KO) mice in Nx (gray) and Hx2 (pink) or Hx3 (blue). For all scatter plots, individual values for females (triangles) and males (circles) are shown, and the black line represents the mean±SEM. The total distribution of mice sex was as follows: (**A**) n=22 females and n=31 males, (**B**) n=20 females and n=33 males, (**C**) n=19 females and n=33 males, (**D**) n=22 females and n=33 males, (**E**) n=23 females and n=35 males, (**G**) n=48 females and n=73 males, and (**I**) n=13 females and n=12 males. Statistical significance was determined using a 1-way ANOVA multiple comparisons test with Tukey correction. Significant *P* values >0.001 are explicitly indicated, while *P* values <0.001 state as *P*<0.001. Nonsignificant (*P*>0.05) *P* values are not shown.

fraction (LVEF; Figure 5D) and increased LV end-diastolic volume (LVED Vol; Figure 5E), indicative of cardiac dilatation (Figure 5F). To connect functional parameters with structural adaptations, next, we performed whole-mount organ analysis, finding a progressive increase of the heart weight/body weight ratio in *Hif2/Wt1* cKO mutant mice

relative to controls (Figure 5G). This gradual cardiomegaly in response to chronic hypoxia was further validated by HE staining (Figure 5H).

Considering that Wt1 lineage contributes to some scattered cardiomyocytes,[37] as we further confirmed by lineage tracing (data not shown), we decided to explore whether the absence of *Hif2* could influence cardiomyocyte size upon hypoxia. To this aim, we performed WGA (wheat germ agglutinin) staining in 14- to 15-week-old heart sections from control and *Hif2/Wt1* cKO mice and compared the size of cardiomyocytes in normoxia and after 2 and 3 weeks of exposure to 10% O_2 in both groups (Figure S4). The analysis indicated an ongoing increase in the cardiomyocyte cell area from normoxia to 2 and 3 weeks of hypoxia in both control and *Hif2/Wt1* mutants (Figure 5I). Nevertheless, we did not find significant differences between control and *Hif2/Wt1* cKO mice at any time point, excluding cardiomyocyte cell hypertrophy as the mechanism responsible for the increased cardiomegaly and elevated heart weight/body weight ratio developed by *Hif2/Wt1* mutants after hypoxia.

Overall, these results indicate that deletion of *Hif2* in the Wt1 lineage compromises cardiac adaptation to chronic hypoxia, causing LV systolic dysfunction and enhanced cardiomegaly not due to cardiomyocyte hypertrophy, pointing to a protective role of vascular HIF2 signaling in the heart during adaptation to low oxygen conditions.

HIF2 Signaling Represses Cardiac EC Proliferation and Prevents Microvascular Remodeling During Chronic Hypoxia

Next, we decided to assess whether the increased cardiomegaly of the *Hif2/Wt1* cKO mice during chronic hypoxia could be due to enhanced cardiac hyperplasia. To explore this possibility, we determined the proliferation rate by immunostaining of cardiac sections of control and *Hif2/Wt1* mutants in normoxia or after exposure to 2 and 3 weeks of hypoxia using mitosis markers (PH3 [phospho histone H3] and Ki67) together with WGA to label cardiomyocyte contour and IB4 and ERG for ECs. Image analysis revealed that hypoxia exposure did not influence cardiomyocyte proliferation, but rather promoted mitosis of the microvasculature compartment (Figure 6A). We further confirmed that IB4$^+$ proliferating cells were indeed ERG$^+$ ECs (Figure S5A). Interestingly, EC proliferation followed a dynamic pattern, with a peak after 2 weeks of hypoxia exposure, followed by a drop close to normoxic values after 3 weeks of hypoxia (Figure 6B), suggesting that HIF2 regulates an inhibitory feedback loop to compensate cardiac endothelial proliferation induced by hypoxia. To explore the impact of proliferation in response to hypoxia, we evaluated the integrity of the cardiac capillary network using IB4 to mark the outline of ECs. Our analysis revealed an increase in the capillary area in the *Hif2/Wt1* cKO mice after 2 and 3 weeks of hypoxia that was not observed in the controls or in normoxia conditions (Figure 6C and 6D). This enlargement in the capillary area suggested a higher capillary diameter that was accompanied by a reduction in the capillary density assessed as the number of capillaries per tissue area (Figure 6E).

Surprisingly, and in contrast to our observations in the lungs, FACS analysis using the Rosa-tdTomato/Wt1Cre reporter mice revealed no changes in the total number of Tomato$^+$ cells, but a significant increase in Tomato$^-$ cells in the heart of *Hif2/Wt1* reporter cKO mice after exposure to 2 weeks of hypoxia (Figure 6F and 6G). Furthermore, despite the endothelial proliferation observed at 2 weeks of hypoxia (Figure 6A) in the mutant mice, FACS analyses showed no significant changes in the total number of ECs between *Hif2/Wt1* reporter cKO and the reporter control mice in hypoxia (Figure 6H through 6J). Nevertheless, there is a trend to increase on the total Tomato$^-$ ECs of the *Hif2/Wt1* reporter cKO mice in hypoxia (Figure 6H). In addition, immunofluorescence combining endothelial (ERG and IB4) and mitosis (Ki67) markers together with endogenous Tomato signal of the reporter revealed that the ECs proliferating in the *Hif2/Wt1* reporter cKO mice are indeed Tomato$^-$ (Figure S5B). Similarly, the total PCs from *Hif2/Wt1* reporter cKO mice did not change significantly in hypoxia, whereas the control Tomato$^+$ PCs were reduced. The Tomato$^-$ PCs population did not change in cKO or control mice (Figure 6K through 6M).

In sum, these results indicate that proliferation of cardiac microvascular ECs is increased after 2 weeks of hypoxia and that HIF2 signaling prevents excessive proliferation in sustained low oxygen conditions. Furthermore, lack of HIF2 leads to cardiac capillary dilation, suggesting a protective role of HIF2 against microvascular remodeling and instability in the heart during chronic hypoxia.

Cardiopulmonary Structural Defects of the *Hif2/Wt1* cKO Mice Are Partially Restored Upon 1-Week Reoxygenation

Because the *Hif2/Wt1* cKO mice did not display alterations in basal conditions, next, we wondered whether the cardiac and pulmonary functional and structural defects developed after chronic hypoxia were reversible. First, we analyzed the impact of 1-week reoxygenation on 2- and 3-weeks hypoxia-induced cardiomegaly (Figure 7A), finding that both control and *Hif2/Wt1* cKO mice were able to restore normoxic values of heart weight/body weight ratio (Figure 7B). Moreover, reoxygenation after chronic hypoxia could also correct capillary density (Figure 7C) while capillary caliber remains slightly increased in the *Hif2/Wt1* cKO mice (Figure 7D). Next, we performed echocardiography analysis and determined that hypoxia-induced RV (Figure 7E) and especially LV

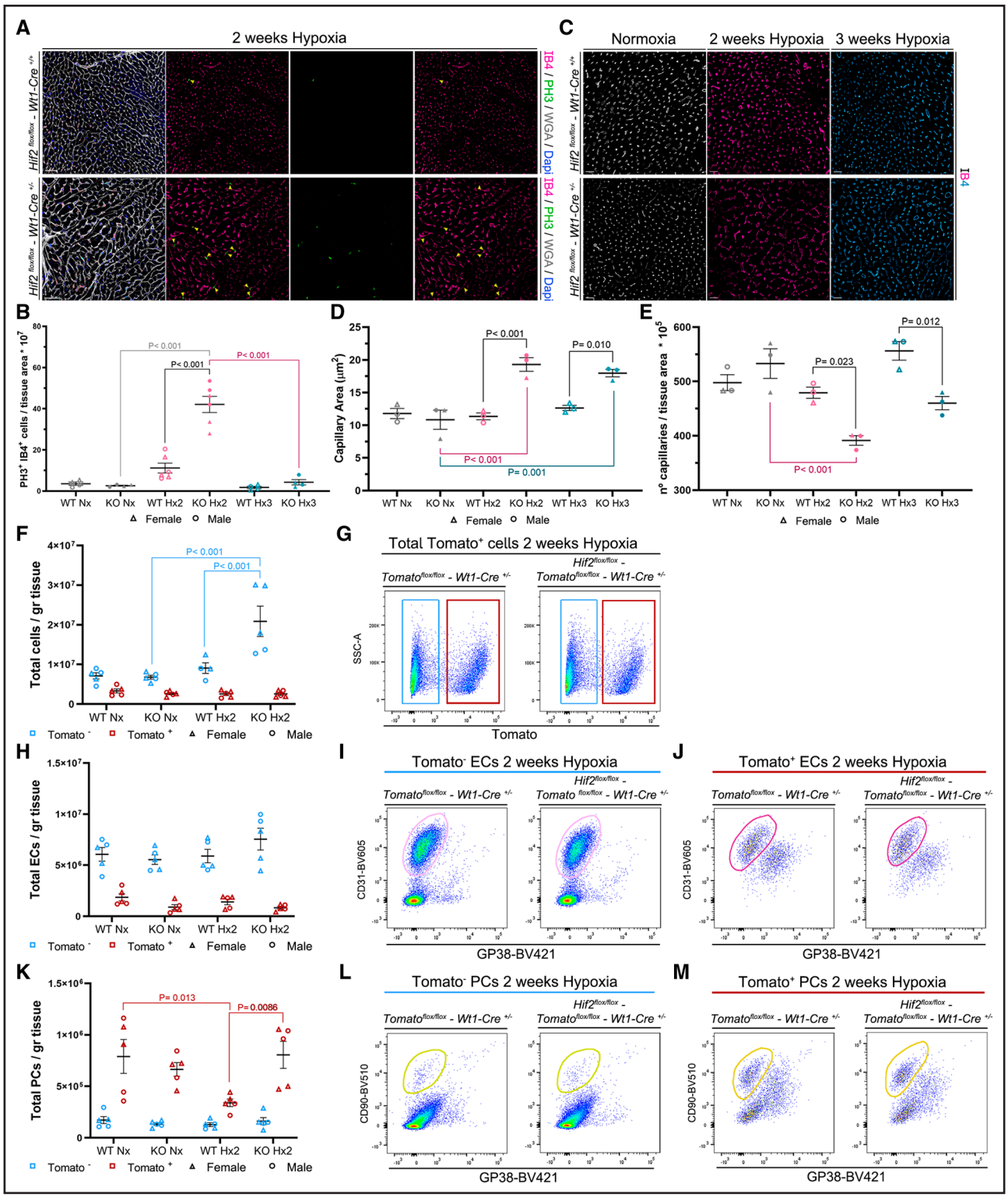

Figure 6. Cardiac microvascular remodeling in response to low oxygen.

A, Immunofluorescence of representative cardiac sections after 2 weeks of hypoxia (Hx2) of control (Hif2$^{flox/flox}$-Wt1-Cre$^{+/+}$, **top**) and *Hif2/Wt1* cKO (conditional knockout) mice (Hif2$^{flox/flox}$-Wt1-Cre$^{+/-}$, **bottom**) with IB4 (isolectin B4; outline of endothelial cells [ECs], magenta), WGA (wheat germ agglutinin; outline of all cells, white), PH3 (phospho histone H3; mitosis, green), and DAPI (4′,6-diamidino-2-phenylindole; nucleus, blue). Yellow arrowheads indicate IB4^{+}/PH3^{+} cells. Scale bars=40 µm. **B**, Quantification of the EC proliferation rate per tissue area in controls (WT [wild type]) and *Hif2* mutants (KO [knockout]) in normoxia (Nx; gray) and Hx2 (pink) or 3 weeks of hypoxia (Hx3; blue). **C**, Representative images of IB4 immunofluorescence of control (Hif2$^{flox/flox}$-Wt1-Cre$^{+/+}$, **top**) and *Hif2/Wt1* cKO mice (Hif2$^{flox/flox}$-Wt1-Cre$^{+/-}$, **bottom**) in Nx (**left**), Hx2 (**middle**), and Hx3 (**right**). Scale bars=20 µm. **D** and **E**, Scatter dot plots for the quantification of the capillary area (**D**) and density (**E**, number of capillaries per tissue area) of controls (WT) and *Hif2* mutants (KO) in Nx (gray), Hx2 (pink), or Hx3 (blue). (*Continued*)

(Figure 7F) hypertrophy returned to normoxia values in the *Hif2/Wt1* cKO mutant mice after 1-week reoxygenation. Furthermore, lung ultrasound revealed restoration of the pulmonary structure on *Hif2/Wt1* cKO mutants after reoxygenation (Figure 7G), with normalization of the pleural thickness and abnormal B/Z band pattern observed after 3 weeks of chronic hypoxia (Figure 3C). The lung ultrasound analysis was further validated by classical histology showing almost complete rescue (Figure 7H) of the pulmonary congestion developed by *Hif2/Wt1* cKO mice after 3 weeks of sustained hypoxia (Figure 3D through 3F).

Nevertheless, despite of these structural improvements on the heart of *Hif2/Wt1* cKO mice upon 1-week reoxygenation after 2 and 3 weeks of hypoxia, the functional parameters were not fully recovered and the *Hif2/Wt1* mutants still displayed reduced LV ejection fraction (Figure 7I), as well as elevated LV end-diastolic volume (Figure 7J), reflecting compromised systolic function and increased cardiac dilatation, respectively.

Altogether, these results demonstrate that HIF2 signaling in the Wt1 lineage is important to maintain the correct cardiopulmonary function and structure of the microvasculature after chronic hypoxia, and that the pathological changes of mice deficient for HIF2 in Wt1-contributed vascular compartments are hypoxia-dependent and reversible in contact with normal oxygen tensions.

DISCUSSION

Sustained hypoxia occurring in patients with cardiorespiratory diseases and at high altitude is associated with profound vascular remodeling due to muscularization of the small arteries of the alveolar wall and proliferation of cells expressing SMA, followed by thickening of the precapillary pulmonary arteries, inflammation, and fibrosis of the large proximal pulmonary arteries, leading to arterial occlusion and elevation of the RVSP.[54] It has been demonstrated that this vascular remodeling and cardiac overload also occurs in rodents, allowing the use of experimental animals exposed to low oxygen as a reliable model to study PH and cardiovascular alterations during chronic hypoxia. Endothelial HIF2 signaling has been extensively implicated in the progression of arterial remodeling, leading to elevated RVSP during sustained hypoxia,[17–19,22] while deletion of HIF2 in SMCs or PCs does not prevent vascular muscularization.[22,23]

In this study, we characterized a novel mouse model, *Hif2/Wt1* cKO mice, to evaluate the impact of lacking HIF2 signaling during chronic hypoxia in several vascular cell types of the cardiopulmonary system, including ECs, PCs , VSMCs, and FBs (Figure 1G through 1M). This lineage contribution allows us to investigate the consequences of simultaneously deleting HIF2 in pulmonary and cardiac vascular cell populations, which could serve as an indicator of the potential effects of systemic HIF2 abrogation with small molecules recently proposed as alternative therapeutic approaches for PH.[24,25] Furthermore, we performed detailed functional and structural characterizations of this new mouse model to better understand the relevance of vascular HIF2 signaling during the cardiovascular response to chronic hypoxia, which to the date remained elusive. We demonstrated that HIF2 signaling in the Wt1 lineage is not necessary for proper development of the heart or lungs, or for organ homoeostasis of adult mice (Figure S2). Furthermore, in agreement with former works, we also observed that elimination of HIF2 in the pulmonary vasculature prevents arterial muscularization and elevation of RV overload (Figure 2). However, the lack of HIF2 in the Wt1 lineage compromises the proper adaptation of the heart and lungs to chronic hypoxia, resulting in microvascular remodeling and dysfunction of both organs. In the lungs, we observed severe hemorrhages, inflammation, and congestion that might be caused by an increased venous return associated with reduced LV ejection fraction and increased LV dilatation (Figure 5), as well as by local microvascular instability (Figures 3 and 4). In the heart, despite the absence of a hemorrhagic phenotype, mutant mice display cardiomegaly, ventricular hypertrophy without significant changes in the cardiomyocyte area, and cardiac failure (Figure 4), most likely due to EC dysfunction associated with capillary dilation (Figure 5). Interestingly, most of these structural defects are restored upon reoxygenation of hypoxia-exposed *Hif2/Wt1* cKO mice, suggesting the existence of inhibitory protective roles mediated by HIF2 signaling in the cardiopulmonary vasculature that only operates in hypoxia (Figure 7). Based on these results, we proposed a working model highlighting the importance of vascular HIF2 signaling for proper

Figure 6 Continued. **F** through **M**, FACS (Fluorescence-Activated Cell Sorting) analysis with Rosa-tdTomato/Wt1 reporter control (WT) and Rosa-tdTomato/Hif2 reporter cKO (KO) mice in Nx and after Hx2. **F**, **H**, and **K**, Scatter dot plots showing Tomato$^-$ (blue) and Tomato$^+$ (red) total cardiac cells (**F**), ECs (**H**), and PCs (pericytes; **K**) per gram (gr) of tissue. **G**, **I**, **J**, **L**, and **M**, Representative FACS pseudocolor plots of control (Tomato$^{flox/flox}$/Wt1$^{+/-}$) and mutant (Tomato$^{flox/flox}$/Hif2$^{flox/flox}$/Wt1$^{+/-}$) mice. All gates were generated from a fixed number of 34 000 CD (cluster of differentiation) 45$^-$ cells. **G**, Total CD45$^-$ cells separating Tomato$^-$ cells (blue gate) and Tomato$^+$ cells (red gate). Tomato$^-$ ECs (purple gates, **I**) and Tomato$^+$ ECs (purple gates, **J**) or Tomato$^-$ PCs (yellow gates, **L**) and Tomato$^+$ PCs (yellow gates, **M**). For all scatter plots, individual values for females (triangles) and males (circles) are shown, and the black line represents the mean±SEM. The total distribution of mice sex was as follows: (**B**) n=14 females and n=14 males, (**D** and **E**) n=8 females and n=10 males, and (**F**, **H**, and **K**) n=21 females and n=18 males. Statistical significance was determined using a 1-way ANOVA multiple comparisons test with Tukey correction. Significant *P* values >0.001 are explicitly indicated, while *P* values <0.001 state as *P*<0.001. Nonsignificant (*P*>0.05) *P* values are not shown. BV421 indicates brilliant violet 421; BV510, brilliant violet 510; BV605, brilliant violet 605; and SSC-A, side scatter-area.

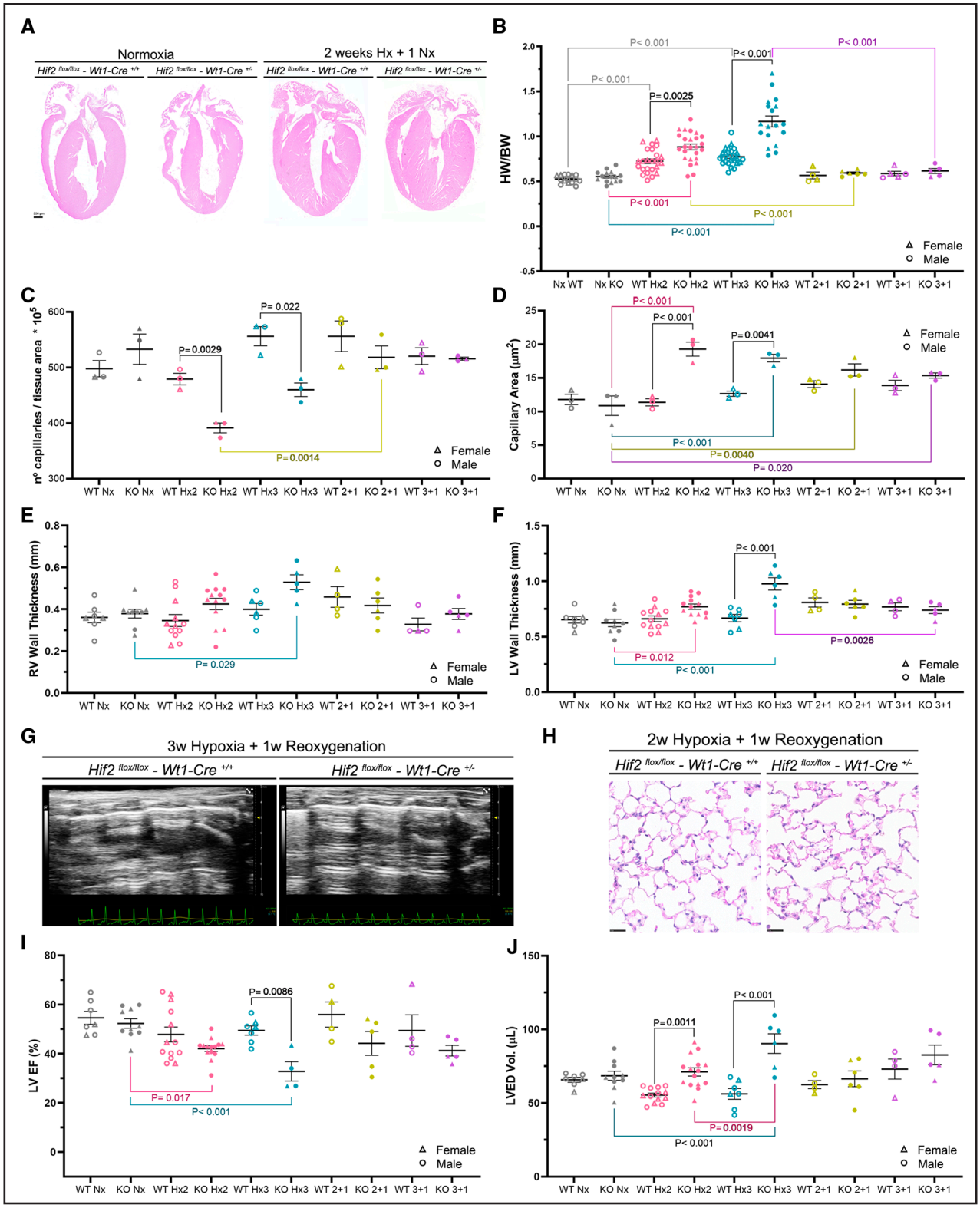

Figure 7. Partial rescue of chronic hypoxia–induced cardiac and pulmonary defects upon reoxygenation.
A, Histological analysis by hematoxylin and eosin (HE) staining of representative heart sections of control (Hif2$^{flox/flox}$-Wt1-Cre$^{+/+}$, **left** panel of each experimental condition) and *Hif2/Wt1* cKO, (conditional knockout) mice (Hif2$^{flox/flox}$-Wt1-Cre$^{+/-}$, **right** panel of each experimental condition) in normoxia (Nx; **left** columns) and 2 weeks of hypoxia followed by 1-week reoxygenation (2 weeks of Hx [Hx2]+1 week of Nx, **right** columns). Scale bar=500 µm. **B**, Quantification of the heart size estimation represented as heart weight/body weight ratio (HW/BW) in control (WT [wild-type]) and *Hif2/Wt1* cKO (conditional knockout) (KO [knockout]) mice in Nx (gray), Hx2 (pink) or 3 weeks of hypoxia (Hx3; blue), and Hx2 or Hx3 followed by 1-week reoxygenation (2+1 [yellow] and 3+1 [purple], respectively). **C** and **D**, Scatter dot plot of density (**C**) and capillary area (**D**) in control (WT) and *Hif2/Wt1* cKO (KO) mice in Nx (gray), Hx2 (pink), or Hx3 (blue), and Hx2 or Hx3 followed by 1-week (*Continued*)

capillary stability and organ performance during cardiac and pulmonary adaptation to chronic hypoxia (Figure 8).

HIF2 global deletion protects against RVSP elevation in response to low oxygen,[55] and later works demonstrated the critical role of EC-HIF2 signaling mediating the vascular remodeling that leads to elevation of RVSP during chronic hypoxia and in PH.[17–19] However, little is known about the role of HIF2 in other cell types within the vascular compartment beyond the endothelium. It has been reported that elimination of HIF2 in SMCs does not prevent RVSP elevation during chronic hypoxia.[22] A recent publication by Kim et al[23] has reported novel mouse models of HIF2 overexpression and deletion in PCs using NG2-CreERT2. Interestingly, while overexpression of HIF2 in PCs leads to elevation of arterial muscularization and increased RVSP after 3 weeks of hypoxia exposure, pointing to an important role of HIF2 signaling from PC mural cells in arterial vascularization, elimination of HIF2 in PCs does not prevent the elevation of RVSP during chronic hypoxia.[23] These results contrast with our findings, showing that the novel *Hif2/Wt1* cKO mice generated in our laboratory are protected against arterial remodeling and elevation of RVSP after hypoxia (Figure 2). Since Wt1 contributes to ECs, PCs , as well as SMCs and fibroblast-like cells of the lung vasculature (Figure 1), one explanation to these contrasting results could be that the protection of *Hif2/Wt1* cKO mice against vascular remodeling in hypoxia was only due to the ablation of HIF2 signaling in the endothelium, which would fully agree with former works.[17–19] Another possibility could be that HIF2 signaling in fibroblast-like cells of the alveolar parenchyma contributed by Wt1 also participates in the arterialization upon hypoxia. Nevertheless, Wt1 contributes to <4% of the total pulmonary FBs (Table S2), and clarifying the precise function of HIF2 in this cell type using alternative mouse models is out of the scope of this article.

Despite the protection against arteriolar remodeling, the *Hif2/Wt1* cKO mice characterized here displayed profound damage of the lung parenchyma after 3 weeks of hypoxia, with reduced alveolar space, inflammation, and hemorrhages, likely due to unstable capillaries and increased remodeling of alveolar microvasculature (Figure 3). These pulmonary tissue alterations have not been reported to the best of our knowledge in the EC-specific models of HIF2 deletion. However, Kim et al[23] have recently reported that the overexpression of HIF2 in PCs induces vascular leakage and disruption of capillary integrity, while the PC-HIF2 KO shows no difference in permeability compared with controls. Taking these results into account, and considering that *Hif2/Wt1* cKO mice developed significant vascular leakage, alveolar hemorrhages, and pulmonary congestion (Figure 3), together with increased EC proliferation, our results suggest that only simultaneous deletion of HIF2 in SMCs/PCs and ECs lead to alveolar vascular defects and lung edema. Alternatively, we cannot rule out that HIF2 deletion in a fibroblast-like interstitial cell type within the alveoli contributed by Wt1 could be responsible for the EC barrier dysfunction observed in our mutants.

While significant works have evaluated the relevance of HIF2 during the adaptation to sustained hypoxia in the lungs, little is known about HIF2 signaling in the heart in response to chronic low oxygen. In the setting of PH, Smith et al[56] explored the possibility that RV hypertrophy after chronic hypoxia might be due not only to the increased load of the right side of the heart upon pulmonary arterial remodeling, but also to pulmonary-independent factors acting directly on the heart that could lead to the activation of HIFs. Indeed, Smith et al[56] demonstrated that both HIF1 and HIF2 signaling on cardiomyocytes is involved in RV hypertrophy during chronic hypoxia. In the *Hif2/Wt1* cKO mutants described here, we also demonstrated direct cardiac alterations most likely independent of the pulmonary defects occurring during chronic hypoxia. This statement is supported by the fact that *Hif2/Wt1* cKO mice developed not only RV but also LV hypertrophy, LV systolic dysfunction based on the reduced LV ejection fraction, and LV dilation (Figure 4). Moreover, considering that Wt1 contributes to capillaries of both RV and LV (Figure 1) and that we did not observe significant differences between *Hif2/Wt1* cKO and control cardiomyocyte area in hypoxia (Figure 4), we hypothesize that the increased RV and LV wall thickness and cardiomegaly observed in the absence of HIF2 might be due to the profound microvascular remodeling and capillary dilation

Figure 7 Continued. reoxygenation (2+1 [yellow] and 3+1 [purple], respectively). **E** and **F**, Quantification of echocardiography analysis to asses cardiac hypertrophy by RV (right ventricular; **E**) and LV (left ventricular; **F**) wall thickness of control (WT) and *Hif2/Wt1* cKO (KO) mice in Nx (gray), Hx2 (pink), or Hx3 (blue), and Hx2 or Hx3 followed by 1-week reoxygenation (2+1 [yellow] and 3+1 [purple], respectively). **G**, Representative images of pulmonary ultrasound in control (Hif2$^{flox/flox}$-Wt1-Cre$^{+/+}$, **left**) and *Hif2/Wt1* cKO mice (Hif2$^{flox/flox}$-Wt1-Cre$^{+/-}$, **right**) after Hx3 followed by 1-week reoxygenation. **H**, Histological analysis by HE of representative lung sections in control (Hif2$^{flox/flox}$-Wt1-Cre$^{+/+}$, **left**) and *Hif2/Wt1* cKO mice (Hif2$^{flox/flox}$-Wt1-Cre$^{+/-}$, **right**) after Hx2 and 1-week reoxygenation. Scale bars=25 µm. **I** and **J**, Functional and structural cardiac parameters assessed by echocardiography of control (WT) and *Hif2/Wt1* cKO (KO) mice in Nx (gray), Hx2 (pink), or Hx3 (blue), and Hx2 or Hx3 followed by 1-week reoxygenation (2+1 [yellow] and 3+1 [purple], respectively). Left ventricular ejection fraction (LVEF; **I**) and left ventricular end-diastolic volume (LVED vol; **J**). For all scatter plots, individual values for females (triangles) and males (circles) are shown, and the black line represents the mean±SEM. The total distribution of mice sex was as follows: (**B**) n=58 females and n=83 males, (**C** and **D**) n=13 females and n=17 males, (**E**) n=27 females and n=44 males, (**F**) n=26 females and n=48 males, (**I**) n=27 females and n=46 males, and (**J**) n=26 females and n=48 males. Statistical significance was determined using a 1-way ANOVA multiple comparisons test with Tukey correction. Significant *P* values >0.001 are explicitly indicated, while *P* values <0.001 state as *P*<0.001. Nonsignificant (*P*>0.05) *P* values are not shown.

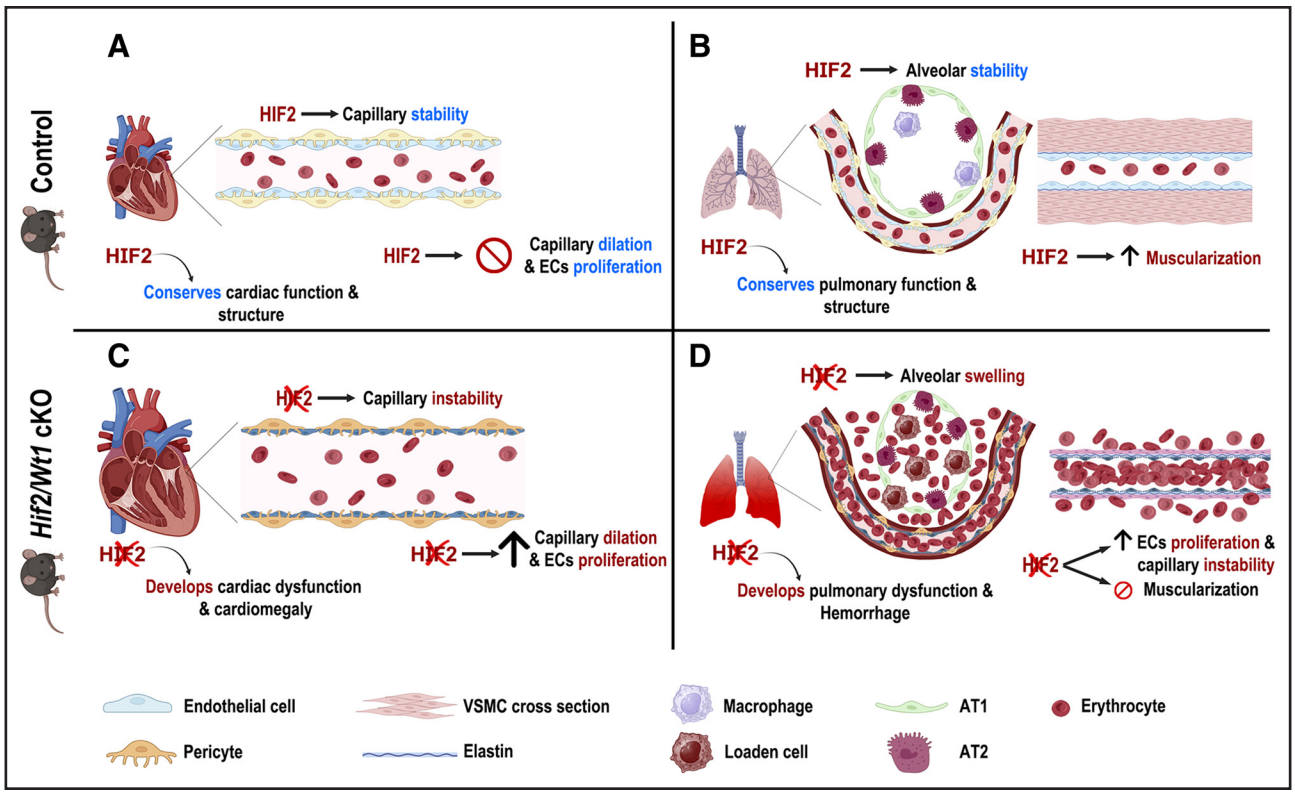

Figure 8. Working model.

Proposed model of cardiopulmonary defects in control and *Hif2/Wt1* cKO (conditional knockout) mice after 3 weeks of chronic hypoxia. Control mice after 3 weeks of hypoxia exposure are protected against cardiomegaly, dilation of capillaries, and increased proliferation of endothelial cells (ECs; **A**), while *Hif2/Wt1* cKO mice develop cardiomegaly associated with capillary dilation and EC proliferation (**C**). Control mice lungs display normal alveolar parenchyma as wild-type HIF2 (hypoxia inducible factor 2) prevents microvascular proliferation, but show HIF2-mediated muscularization of the distal arterioles and increased right ventricular systolic pressure (RVSP; **B**). In contrast, *Hif2/Wt1* cKO mice are protected against arterial muscularization but present several structural lung defects, including erythrocytes and macrophages congestion, hemorrhages, and alveolar wall thickening, probably associated to alveolar capillary remodeling and proliferation (**D**). Altogether, these results suggest that HIF2 plays an inhibitory role upon cardiac and pulmonary ECs, pericytes (PCs), and vascular smooth muscle cells (VSMCs) that prevents excessive microvascular remodeling and organ dysfunction in response to chronic hypoxia. AT1 indicates alveolar type I; and AT2, alveolar type II.

observed in these mutants (Figure 4). Interestingly, the recently reported HIF2/NG2 KO model does not exhibit ventricular hypertrophy, fibrosis, or cardiac dysfunction in response to chronic hypoxia,[23] suggesting that the vascular alterations developed by the *Hif2/Wt1* cKO mice might be due to the lack of functional HIF2 signaling in microvascular endothelium rather than in cardiac PCs during low oxygen exposure. It is important to mention that in contrast with the cardiomyocyte-specific HIF2 mutant,[56] the *Hif2/Wt1* cKO mice described here developed systolic dysfunction (Figure 4), while both mutants undergo ventricular dilation. These results highlight the importance of functional HIF2 signaling in the vascular compartment of the heart to ensure proper functional adaptation to sustained hypoxia. Hence, our data further contribute to increase our limited understanding on the cardiac intrinsic response to hypoxia independently of pulmonary remodeling.

Several studies have demonstrated the role of endothelial HIF2 in the vascular remodeling of pulmonary arteries within the pathogenesis of PH,[17–19] and recent therapeutic targeting of HIF2 with small molecule inhibitors, such as PT-2567, has shown a beneficial effect preventing the initiation of PH in rat models.[24,25] Nevertheless, the detailed consequences of prolonged systemic inhibition of HIF2 signaling in other organs essential for physiological homeostasis, like the heart, remain elusive and have not been reported in detail in previous works. In this study, the use of a genetic approach that allows the simultaneous deletion of HIF2 in several cell types of the vasculature, like ECs and SMCs, as well as PCs and FBs , offered us the advantage of evaluating a plethora of cells involved in PH progression and exploring potential effects associated with the systemic abrogation of HIF2 in the heart and lungs. Even though the relative inhibition of HIF2 signaling using PT-2567 in rat models of PH could prevent pulmonary vascular remodeling, as well as circulating proinflammatory factors and plasma nitrite levels,[24,25] it is important to mention that our mouse model also displayed a decrease on RVSP and reduced pulmonary remodeling. Despite these clear beneficial effects of lacking HIF2 to prevent the initiation of PH, the whole impact of loosing HIF2 signaling during the adaptation to chronic hypoxia has not been previously

addressed in mouse models. In fact, our results show that concomitant elimination of HIF2 in several vascular cell types involved in PH disease leads to structural and functional abnormalities in both heart and lungs, including pulmonary inflammation, hemorrhages, erythroid extravasation, and alveolar congestion, as well as cardiomegaly, ventricular hypertrophy, and systolic dysfunction associated with capillary remodeling and dilation under low oxygen conditions.

Therefore, our data describe novel cardiac and pulmonary phenotypic characteristics of HIF2 abrogation and uncover unknown protective roles of HIF2 signaling in the microvasculature of the heart and lungs, suggesting that HIF2 is essential to avoid excessive EC proliferation, ensuring stable microvascular networks in both organs during sustained exposure to hypoxia. These observations were not anticipated based on the protection of the *Hif2/Wt1* cKO mice against pulmonary arterial remodeling and elevation of RVSP, but are in line with former studies reporting that despite the reduced vascular remodeling, global genetic deletion of HIF2α or systemic inhibition using antisense oligos impairs survival upon 4 weeks of hypoxia exposure,[24] leading to weight loss and reduced catecholamine levels, heart rate, and cardiac output, probably reflecting the critical importance of HIF2 in organs like the carotid body to ensure proper hypoxia adaptation.

Hence, based on the heterogeneous and diverse relevance of HIF2 depending on the cellular/organ context, further studies will be required to better characterize the global consequences of systemic inhibition of HIF2 to define novel alternative therapeutic strategies able to blunt HIF2 detrimental effects without precluding its beneficial role in other cell types or tissues. In that regard, the design of endothelial-specific delivery vectors to limit the action of HIF2 inhibitors to this cell type, which is clearly involved in the initiation of PH,[17–19,24,25] would contribute to minimize deleterious effects in nonendothelial compartments. Our work contributes to expand our limited knowledge on the role of vascular HIF2 signaling in the cardiovascular system and might be relevant to evaluate potential long-term effects in the setting of HIF2-specific inhibitory therapies recently approved for renal clear cell carcinoma[57] and proposed for PH,[24,25] especially in patients with lung conditions who might experience chronic hypoxia.

ARTICLE INFORMATION

Received August 29, 2024; accepted January 2, 2025.

Affiliations

Metabolic and Immune Diseases Department, Instituto de Investigaciones Biomedicas Sols-Morreale (IIBM), CSIC-UAM, Madrid, Spain (T.A.-G., S.M.-T., R.C.-M., S.U.-B., S.M.-P.). Cardiovascular Regeneration Program, Centro Nacional de Investigaciones Cardiovasculares, Carlos III (CNIC), Madrid, Spain (T.A.-G., S.M.-T., B.E., S.F.R., J.A.N.-A., E.O., M.V.-O., S.M.-P.). School of Medicine, Universidad Francisco de Vitoria, Madrid, Spain (T.A.-G., S.M.-P.). Mouse Genome Editing Unit, Centro Nacional de Investigaciones Oncológicas (CNIO), Madrid, Spain (B.E.). Cardiovascular Research Institute & Department of Microbiology and Immunology, University of California San Francisco (J.A.N.-A.). Biomedicine Department, Centro de Investigaciones Biológicas Margarita Salas (CIB), Madrid, Spain (E.O.). Centro de Investigación Biomédica en Red de Enfermedades Cardiovasculares, Spain (E.O.). Department of Animal Medicine and Surgery, Universidad Complutense de Madrid, Madrid, Spain (M.V.-O.). Centro de Investigación Biomédica en Red de Enfermedades Respiratorias, Spain (S.M.-P.).

Acknowledgments

The authors thank Jose Luis de La Pompa for the Wt1-Cre mouse line. They acknowledge Virginia García, Eva Garrido, Raquel Álvarez, and Mercedes de la Cueva for animal housing and handling, Antonio de Molina for histopathologic analysis, Elena Prieto for assistance on FACS (Fluorescence-activated cell sorting) analysis and sorting, and CNIC (Centro Nacional de Investigaciones Cardiovasculares) Microscopy and Dynamic Imaging (ICTS-ReDib, Infraestructuras Científico-Tecnológicas Singulares-Red Distribuida de Imagen Biomédica, cofounded by MCIN/AEI/10.13039/50110001103), CellomicsCore Facility, and Histology Core Facility for technical assistance. They thank Mónica M.-Belinchón and Barbara Acosta Iborra of Servicio de Microscopía Óptica y Confocal del IIBM (Instituto de Investigaciones Biomedicas Sols-Morreale) for microscopy assistance and Diana Muñoz for technical support. T. Albendea-Gomez performed most of the experiments, analyzed data, made the figures, and helped to write the manuscript. M. Villalba-Orero performed echocardiography and lung ultrasound analysis and discussed the manuscript. J.A. Nicolas-Avila contributed to FACS analysis and gating strategy and discussed the manuscript. S.F. Rocha and E. Oliver performed right ventricular systolic pressure measurements and E. Oliver discussed the manuscript. S. Mendoza-Tamajon, B. Escobar, R. Castro-Mecinas, and S. Urra-Balduz supported the experiments. S. Martin-Puig defined the concept, planned and supervised experiments, analyzed data, wrote the manuscript, designed the figures together with T. Albendea-Gomez, and obtained funding to support the study. The authors declare that no artificial intelligence (AI) or AI-assisted technologies were applied to generate this article.

Sources of Funding

This project has been supported by grants to S. Martin-Puig (SMP) from Universidad Francisco de Vitoria (UFV), LeDucq Foundation: 17CVD04, the Spanish Ministry of Science and Innovation (Ministerio de Ciencia, Innovación y Universidades, MICIU): PID2020-117629RB-I00/AEI/10.13039/501100011033, Comunidad de Madrid (CM): S2022/BMD-7245 (CARDIOBOOST-CM), and Fundación Domingo Martínez: "Ayuda de Biomedicina 2023." T. Albendea-Gomez was supported by a predoctoral award granted by CM/EU (European Union) and UFV: PEJD-2018-PRE/SAL-9529 and SMP project PID2020-117629RB-I00/AEI/10.13039/501100011033. S. Mendoza-Tamajon was funded by a predoctoral contract from the Spanish Ministry of Science and Innovation and European Regional Development Fund: PRE-2021-099445. R. Castro-Mecinas was funded by a contract from CM: PEJ-2021-AI/BMD-21926. B. Escobar was supported by SMP project 17CVD04. S. Urra-Balduz was funded by SMP project S2022/BMD-7245. J.A. Nicolas-Avila was supported by the University of California San Francisco (UCSF) Cardiovascular Research Institute department, the UCSF Dean's office program, and the Young Investigator Competitive Award from the International Society for Heart Research. M. Villalba-Orero was funded by a Juan de la Cierva Incorporación Grant (IJCI-2016-27698). E. Oliver received funding from MICIU PID2021-123167OB-I00. E. Oliver and S. Martin-Puig were supported by the Spanish National Research Council (CSIC).

Disclosures

None.

Supplemental Material

Supplemental Methods
Tables S1–S4
Figures S1–S5
Major Resources Tables

REFERENCES

1. Simon MC, Keith B. The role of oxygen availability in embryonic development and stem cell function. *Nat Rev Mol Cell Biol.* 2008;9:285–296. doi: 10.1038/nrm2354
2. Kaelin WG Jr, Ratcliffe PJ. Oxygen sensing by metazoans: the central role of the HIF hydroxylase pathway. *Mol Cell.* 2008;30:393–402. doi: 10.1016/j.molcel.2008.04.009

3. Majmundar AJ, Wong WJ, Simon MC. Hypoxia-inducible factors and the response to hypoxic stress. *Mol Cell*. 2010;40:294–309. doi: 10.1016/j.molcel.2010.09.022
4. Dengler VL, Galbraith M, Espinosa JM. Transcriptional regulation by hypoxia inducible factors. *Crit Rev Biochem Mol Biol*. 2014;49:1–15. doi: 10.3109/10409238.2013.838205
5. Koh MY, Powis G. Passing the baton: the HIF switch. *Trends Biochem Sci*. 2012;37:364–372. doi: 10.1016/j.tibs.2012.06.004
6. Hu CJ, Wang LY, Chodosh LA, Keith B, Simon MC. Differential roles of hypoxia-inducible factor 1alpha (HIF-1alpha) and HIF-2alpha in hypoxic gene regulation. *Mol Cell Biol*. 2003;23:9361–9374. doi: 10.1128/MCB.23.24.9361-9374.2003
7. Mole DR, Blancher C, Copley RR, Pollard PJ, Gleadle JM, Ragoussis J, Ratcliffe PJ. Genome-wide association of hypoxia-inducible factor (HIF)-1alpha and HIF-2alpha DNA binding with expression profiling of hypoxia-inducible transcripts. *J Biol Chem*. 2009;284:16767–16775. doi: 10.1074/jbc.M901790200
8. Knutson AK, Williams AL, Boisvert WA, Shohet RV. HIF in the heart: development, metabolism, ischemia, and atherosclerosis. *J Clin Invest*. 2021;131:e137557. doi: 10.1172/JCI137557
9. Krishnan J, Ahuja P, Bodenmann S, Knapik D, Perriard E, Krek W, Perriard J-C. Essential role of developmentally activated hypoxia-inducible factor 1alpha for cardiac morphogenesis and function. Research support, non-U.S. gov't. *Circ Res*. 2008;103:1139–1146. doi: 10.1161/01.RES.0000338613.89841.c1
10. Guimaraes-Camboa N, Stowe J, Aneas I, Sakabe N, Cattaneo P, Henderson L, Kilberg MS, Johnson RS, Chen J, McCulloch AD, et al. HIF1alpha represses cell stress pathways to allow proliferation of hypoxic fetal cardiomyocytes. *Dev Cell*. 2015;33:507–521. doi: 10.1016/j.devcel.2015.04.021
11. Menendez-Montes I, Escobar B, Gomez MJ, Albendea-Gomez T, Palacios B, Bonzon-Kulichenko E, Izquierdo-Garcia JL, Alonso AV, Ferrarini A, Jimenez-Borreguero LJ, et al. Activation of amino acid metabolic program in cardiac HIF1-alpha-deficient mice. *iScience*. 2021;24:102124. doi: 10.1016/j.isci.2021.102124
12. Menendez-Montes I, Escobar B, Palacios B, Gómez MJ, Izquierdo-Garcia JL, Flores L, Jiménez-Borreguero LJ, Aragones J, Ruiz-Cabello J, Torres M, et al. Myocardial VHL-HIF signaling controls an embryonic metabolic switch essential for cardiac maturation. *Dev Cell*. 2016;39:724–739. doi: 10.1016/j.devcel.2016.11.012
13. Tian H, Hammer RE, Matsumoto AM, Russell DW, McKnight SL. The hypoxia-responsive transcription factor EPAS1 is essential for catecholamine homeostasis and protection against heart failure during embryonic development. *Genes Dev*. 1998;12:3320–3324. doi: 10.1101/gad.12.21.3320
14. Scortegagna M, Ding K, Oktay Y, Gaur A, Thurmond F, Yan L-J, Marck BT, Matsumoto AM, Shelton JM, Richardson JA, et al. Multiple organ pathology, metabolic abnormalities and impaired homeostasis of reactive oxygen species in Epas1-/- mice. *Nat Genet*. 2003;35:331–340. doi: 10.1038/ng1266
15. Peng J, Zhang L, Drysdale L, Fong GH. The transcription factor EPAS-1/hypoxia-inducible factor 2alpha plays an important role in vascular remodeling. *Proc Natl Acad Sci USA*. 2000;97:8386–8391. doi: 10.1073/pnas.140087397
16. Shimoda LA, Semenza GL. HIF and the lung: role of hypoxia-inducible factors in pulmonary development and disease. *Am J Respir Crit Care Med*. 2011;183:152–156. doi: 10.1164/rccm.201009-1393PP
17. Kapitsinou PP, Rajendran G, Astleford L, Michael M, Schonfeld MP, Fields T, Shay S, French JL, West J, Haase VH. The endothelial prolyl-4-hydroxylase domain 2/hypoxia-inducible factor 2 axis regulates pulmonary artery pressure in mice. *Mol Cell Biol*. 2016;36:1584–1594. doi: 10.1128/MCB.01055-15
18. Dai Z, Li M, Wharton J, Zhu MM, Zhao YY. Prolyl-4 hydroxylase 2 (PHD2) deficiency in endothelial cells and hematopoietic cells induces obliterative vascular remodeling and severe pulmonary arterial hypertension in mice and humans through hypoxia-inducible factor-2alpha. *Circulation*. 2016;133:2447–2458. doi: 10.1161/CIRCULATIONAHA.116.021494
19. Cowburn AS, Crosby A, Macias D, Branco C, Colaço RDDR, Southwood M, Toshner M, Crotty Alexander LE, Morrell NW, Chilvers ER, et al. HIF2alpha-arginase axis is essential for the development of pulmonary hypertension. *Proc Natl Acad Sci USA*. 2016;113:8801–8806. doi: 10.1073/pnas.1602978113
20. Kurakula K, Smolders V, Tura-Ceide O, Jukema JW, Quax PHA, Goumans MJ. Endothelial dysfunction in pulmonary hypertension: cause or consequence? *Biomedicines*. 2021;9:57. doi: 10.3390/biomedicines9010057
21. Sheikh AQ, Saddouk FZ, Ntokou A, Mazurek R, Greif DM. Cell autonomous and non-cell autonomous regulation of SMC progenitors in pulmonary hypertension. *Cell Rep*. 2018;23:1152–1165. doi: 10.1016/j.celrep.2018.03.043
22. Tang H, Babicheva A, McDermott KM, Gu Y, Ayon RJ, Song S, Wang Z, Gupta A, Zhou T, Sun X, et al. Endothelial HIF-2alpha contributes to severe pulmonary hypertension due to endothelial-to-mesenchymal transition. *Am J Physiol Lung Cell Mol Physiol*. 2018;314:L256–L275. doi: 10.1152/ajplung.00096.2017
23. Kim H, Liu Y, Kim J, Kim Y, Klouda T, Fisch S, Baek SH, Liu T, Dahlberg S, Hu CJ, et al. Pericytes contribute to pulmonary vascular remodeling via HIF2alpha signaling. *EMBO Rep*. 2024;25:616–645. doi: 10.1038/s44319-023-00054-w
24. Macias D, Moore S, Crosby A, Southwood M, Du X, Tan H, Xie S, Vassallo A, Wood AJT, Wallace EM, et al. Targeting HIF2alpha-ARNT heterodimerisation as a novel therapeutic strategy for pulmonary arterial hypertension. *Eur Respir J*. 2021;57:1902061. doi: 10.1183/13993003.02061-2019
25. Hu CJ, Poth JM, Zhang H, Flockton A, Laux A, Kumar S, McKeon B, Mouradian G, Li M, Riddle S, et al. Suppression of HIF2 signalling attenuates the initiation of hypoxia-induced pulmonary hypertension. *Eur Respir J*. 2019;54:1900378. doi: 10.1183/13993003.00378-2019
26. Walker AM, Langleben D, Korelitz JJ, Rich S, Rubin LJ, Strom BL, Gonin R, Keast S, Badesch D, Barst RJ, et al. Temporal trends and drug exposures in pulmonary hypertension: an American experience. *Am Heart J*. 2006;152:521–526. doi: 10.1016/j.ahj.2006.02.020
27. Mair KM, Johansen AK, Wright AF, Wallace E, MacLean MR. Pulmonary arterial hypertension: basis of sex differences in incidence and treatment response. *Br J Pharmacol*. 2014;171:567–579. doi: 10.1111/bph.12281
28. Rabinovitch M, Gamble WJ, Miettinen OS, Reid L. Age and sex influence on pulmonary hypertension of chronic hypoxia and on recovery. *Am J Physiol*. 1981;240:H62–H72. doi: 10.1152/ajpheart.1981.240.1.H62
29. White K, Johansen AK, Nilsen M, Ciuclan L, Wallace E, Paton L, Campbell A, Morecroft I, Loughlin L, McClure JD, et al. Activity of the estrogen-metabolizing enzyme cytochrome P450 1B1 influences the development of pulmonary arterial hypertension. *Circulation*. 2012;126:1087–1098. doi: 10.1161/CIRCULATIONAHA.111.062927
30. Lahm T, Albrecht M, Fisher AJ, Selej M, Patel NG, Brown JA, Justice MJ, Brown MB, Van Demark M, Trulock KM, et al. 17β-estradiol attenuates hypoxic pulmonary hypertension via estrogen receptor-mediated effects. *Am J Respir Crit Care Med*. 2012;185:965–980. doi: 10.1164/rccm.201107-1293OC
31. Nadadur RD, Umar S, Wong G, Eghbali M, Iorga A, Matori H, Partow-Navid R, Eghbali M. Reverse right ventricular structural and extracellular matrix remodeling by estrogen in severe pulmonary hypertension. *J Appl Physiol (1985)*. 2012;113:149–158. doi: 10.1152/japplphysiol.01349.2011
32. Wilm B, Munoz-Chapuli R. The role of WT1 in embryonic development and normal organ homeostasis. *Methods Mol Biol*. 2016;1467:23–39. doi: 10.1007/978-1-4939-4023-3_3
33. Munoz-Chapuli R, Macias D, Gonzalez-Iriarte M, Carmona R, Atencia G, Perez-Pomares JM. [The epicardium and epicardial-derived cells: multiple functions in cardiac development]. *Rev Esp Cardiol*. 2002;55:1070–1082. doi: 10.1016/s0300-8932(02)76758-4
34. Martinez-Estrada OM, Lettice LA, Essafi A, Guadix JA, Slight J, Velecela V, Hall E, Reichmann J, Devenney PS, Hohenstein P, et al. Wt1 is required for cardiovascular progenitor cell formation through transcriptional control of Snail and E-cadherin. *Nat Genet*. 2010;42:89–93. doi: 10.1038/ng.494
35. Zhou B, Ma Q, Rajagopal S, Wu SM, Domian I, Rivera-Feliciano J, Jiang D, von Gise A, Ikeda S, Chien KR, et al. Epicardial progenitors contribute to the cardiomyocyte lineage in the developing heart. *Nature*. 2008;454:109–113. doi: 10.1038/nature07060
36. Wagner N, Ninkov M, Vukolic A, Deniz GC, Rassoulzadegan M, Michiels JF, Wagner KD. Implications of the Wilms' tumor suppressor wt1 in cardiomyocyte differentiation. *Int J Mol Sci*. 2021;22:4346. doi: 10.3390/ijms22094346
37. Diaz Del Moral S, Barrena S, Hernandez-Torres F, Aránega A, Villaescusa JM, Gómez Doblas JJ, Franco D, Jiménez-Navarro M, Muñoz-Chápuli R, Carmona R. Deletion of the Wilms' tumor suppressor gene in the cardiac troponin-t lineage reveals novel functions of WT1 in heart development. *Front Cell Dev Biol*. 2021;9:683861. doi: 10.3389/fcell.2021.683861
38. Duim SN, Goumans MJ, Kruithof BPT. WT1 in cardiac development and disease. In: van den Heuvel-Eibrink MM, ed. *Wilms Tumor*. 2016.
39. Cano E, Carmona R, Munoz-Chapuli R. Wt1-expressing progenitors contribute to multiple tissues in the developing lung. *Am J Physiol Lung Cell Mol Physiol*. 2013;305:L322–L332. doi: 10.1152/ajplung.00424.2012
40. del Monte G, Casanova JC, Guadix JA, MacGrogan D, Burch JBE, Pérez-Pomares JM, de la Pompa JL. Differential Notch signaling in the epicardium is required for cardiac inflow development and coronary vessel morphogenesis. *Circ Res*. 2011;108:824–836. doi: 10.1161/CIRCRESAHA.110.229062

41. Gruber M, Hu CJ, Johnson RS, Brown EJ, Keith B, Simon MC. Acute postnatal ablation of Hif-2alpha results in anemia. *Proc Natl Acad Sci USA*. 2007;104:2301–2306. doi: 10.1073/pnas.0608382104
42. Zhu X, Bergles DE, Nishiyama A. NG2 cells generate both oligodendrocytes and gray matter astrocytes. *Development*. 2008;135:145–157. doi: 10.1242/dev.004895
43. Villalba-Orero M, Lopez-Olaneta MM, Gonzalez-Lopez E, Padrón-Barthe L, Gómez-Salinero JM, García-Prieto J, Wai T, García-Pavía P, Ibáñez B, Jiménez-Borreguero LJ, et al. Lung ultrasound as a translational approach for non-invasive assessment of heart failure with reduced or preserved ejection fraction in mice. *Cardiovasc Res*. 2017;113:1113–1123. doi: 10.1093/cvr/cvx090
44. Schneider CA, Rasband WS, Eliceiri KW. NIH Image to ImageJ: 25 years of image analysis. *Nat Methods*. 2012;9:671–675. doi: 10.1038/nmeth.2089
45. Skelly DA, Squiers GT, McLellan MA, Bolisetty MT, Robson P, Rosenthal NA, Pinto AR. Single-cell transcriptional profiling reveals cellular diversity and intercommunication in the mouse heart. *Cell Rep*. 2018;22:600–610. doi: 10.1016/j.celrep.2017.12.072
46. Stellato M, Czepiel M, Distler O, Blyszczuk P, Kania G. Identification and isolation of cardiac fibroblasts from the adult mouse heart using two-color flow cytometry. *Front Cardiovasc Med*. 2019;6:105. doi: 10.3389/fcvm.2019.00105
47. Ugorski M, Dziegiel P, Suchanski J. Podoplanin - a small glycoprotein with many faces. *Am J Cancer Res*. 2016;6:370–386.
48. Travaglini KJ, Nabhan AN, Penland L, Sinha R, Gillich A, Sit RV, Chang S, Conley SD, Mori Y, Seita J, et al. A molecular cell atlas of the human lung from single-cell RNA sequencing. *Nature*. 2020;587:619–625. doi: 10.1038/s41586-020-2922-4
49. Zhou B, Pu WT. Genetic Cre-loxP assessment of epicardial cell fate using Wt1-driven Cre alleles. *Circ Res*. 2012;111:e276–e280. doi: 10.1161/CIRCRESAHA.112.275784
50. Horie M, Castaldi A, Sunohara M, Wang H, Ji Y, Liu Y, Li F, Wilkinson TA, Hung L, Shen H, et al. Integrated single-cell RNA-sequencing analysis of aquaporin 5-expressing mouse lung epithelial cells identifies GPRC5A as a novel validated type i cell surface marker. *Cells*. 2020;9:2460. doi: 10.3390/cells9112460
51. Lin C, Song H, Huang C, Yao E, Gacayan R, Xu SM, Chuang PT. Alveolar type II cells possess the capability of initiating lung tumor development. *PLoS One*. 2012;7:e53817. doi: 10.1371/journal.pone.0053817
52. Sorokin SP, Hoyt RF, Jr. Macrophage development: I. Rationale for using Griffonia simplicifolia isolectin B4 as a marker for the line. *Anat Rec*. 1992;232:520–526. doi: 10.1002/ar.1092320409
53. Sheikh AQ, Misra A, Rosas IO, Adams RH, Greif DM. Smooth muscle cell progenitors are primed to muscularize in pulmonary hypertension. *Sci Transl Med*. 2015;7:308ra–30159. doi: 10.1126/scitranslmed.aaa9712
54. Stenmark KR, Meyrick B, Galie N, Mooi WJ, McMurtry IF. Animal models of pulmonary arterial hypertension: the hope for etiological discovery and pharmacological cure. *Am J Physiol Lung Cell Mol Physiol*. 2009;297:L1013–L1032. doi: 10.1152/ajplung.00217.2009
55. Brusselmans K, Compernolle V, Tjwa M, Wiesener MS, Maxwell PH, Collen D, Carmeliet P. Heterozygous deficiency of hypoxia-inducible factor-2alpha protects mice against pulmonary hypertension and right ventricular dysfunction during prolonged hypoxia. *J Clin Invest*. 2003;111:1519–1527. doi: 10.1172/JCI15496
56. Smith KA, Waypa GB, Dudley VJ, Budinger GRS, Abdala-Valencia H, Bartom E, Schumacker PT. Role of hypoxia-inducible factors in regulating right ventricular function and remodeling during chronic hypoxia-induced pulmonary hypertension. *Am J Respir Cell Mol Biol*. 2020;63:652–664. doi: 10.1165/rcmb.2020-0023OC
57. Choi WSW, Boland J, Lin J. Hypoxia-inducible factor-2alpha as a novel target in renal cell carcinoma. *J Kidney Cancer VHL*. 2021;8:1–7. doi: 10.15586/jkcvhl.v8i1.170